Inorg. Chem. **2005**, *44*, 742–757

Forum

Rapid Freeze-Quench ^{57}Fe Mössbauer Spectroscopy: Monitoring Changes of an Iron-Containing Active Site during a Biochemical Reaction

Carsten Krebs,*[,†,‡] John C. Price,[†] Jeffrey Baldwin,[†,§] Lana Saleh,[†] Michael T. Green,*[,‡] and J. Martin Bollinger, Jr.*[,†,‡]

Department of Biochemistry and Molecular Biology and Department of Chemistry, The Pennsylvania State University, University Park, Pennsylvania 16802

Received October 20, 2004

Nuclear gamma resonance spectroscopy, also known as Mössbauer spectroscopy, is a technique that probes transitions between the nuclear ground state and a low-lying nuclear excited state. The nucleus most amenable to Mössbauer spectroscopy is ^{57}Fe, and ^{57}Fe Mössbauer spectroscopy provides detailed information about the chemical environment and electronic structure of iron. Iron is by far the most structurally and functionally diverse metal ion in biology, and ^{57}Fe Mössbauer spectroscopy has played an important role in the elucidation of its biochemistry. In this article, we give a brief introduction to the technique and then focus on two recent exciting developments pertaining to the application of ^{57}Fe Mössbauer spectroscopy in biochemistry. The first is the use of the rapid freeze-quench method in conjunction with Mössbauer spectroscopy to monitor changes at the Fe site during a biochemical reaction. This method has allowed for trapping and subsequent detailed spectroscopic characterization of reactive intermediates and thus has provided unique insight into the reaction mechanisms of Fe-containing enzymes. We outline the methodology using two examples: (1) oxygen activation by the non-heme diiron enzymes and (2) oxygen activation by taurine:α-ketoglutarate dioxygenase (TauD). The second development concerns the calculation of Mössbauer parameters using density functional theory (DFT) methods. By using the example of TauD, we show that comparison of experimental Mössbauer parameters with those obtained from calculations on model systems can be used to provide insight into the structure of a reaction intermediate.

Mössbauer Spectroscopy: General Considerations

^{57}Fe Mössbauer spectroscopy is a nuclear resonance technique that involves transitions between the nuclear ground state, which has $I = {}^1/_2$, and the first excited state ($I = {}^3/_2$), 14.4 keV above the ground state. Decay of the radioactive isotope ^{57}Co (half-life of 270 days) results in the emission of the 14.4-keV photon used for ^{57}Fe Mössbauer spectroscopy (Figure 1A). The emitted 14.4-keV photon can then be absorbed by an ^{57}Fe nucleus in the sample. Because of the laws of conservation of momentum and energy, the emission (absorption) of a γ-photon is associated with a significant recoil, which results in a shift of the energy of the emitted (absorbed) photon. This energy difference (1.95 meV) is ~6 orders of magnitude larger than the line width, which is determined by the lifetime of the excited state of the ^{57}Fe nucleus ($\tau = 143$ ns, corresponding to 4.55 neV). Rudolf Mössbauer showed that, when the emitting and absorbing nuclei are embedded in a solid lattice, there is a certain probability, *f*, for *recoilless* emission or absorption

* To whom correspondence should be addressed: Carsten Krebs, 306 South Frear Laboratory, University Park, PA 16802. Phone: 814-865-6089. Fax: 814-863-7024. E-mail: ckrebs@psu.edu. J. Martin Bollinger, Jr., 208 Althouse Laboratory, University Park, PA 16802. Phone: 814-863-5707. Fax: 814-863-7024. E-mail: jmb21@psu.edu. Michael T. Green, 330 Chemistry Building, University Park, PA 16802. Phone: 814-863-0925. Fax: 814-865-3314. E-mail: mtg10@psu.edu.

† Department of Biochemistry and Molecular Biology.

‡ Department of Chemistry.

§ Present address: Department of Pharmacology, UT Southwestern Medical Center at Dallas, Dallas, Texas 75390.

10.1021/ic048523l CCC: $30.25
Published on Web 02/01/2005

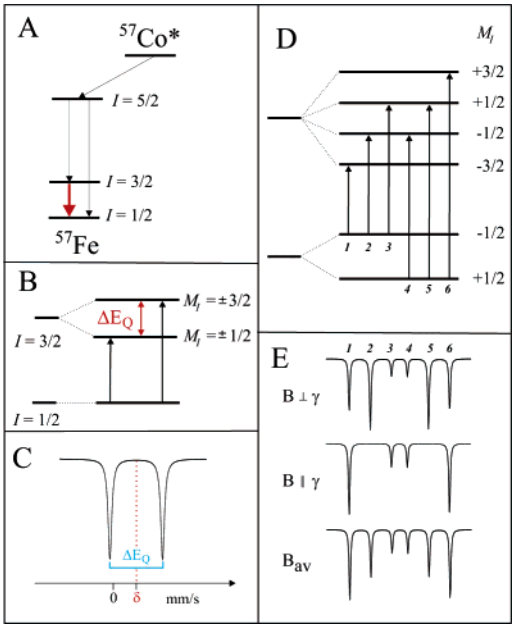

Figure 1. (A) Decay scheme of ^{57}Co. The 14.4-keV transition used for ^{57}Fe Mössbauer spectroscopy is shown in red. (B) Mössbauer transitions without magnetic field. (C) Quadrupole doublet Mössbauer spectrum. (D) Energy levels of the ^{57}Fe states and Mössbauer transitions in the presence of a magnetic field. (E) Magnetic Mössbauer spectra for different orientations of the magnetic field relative to the propagation direction of the γ photon. The quadrupole interaction has been neglected in D and E.

of the γ-photon, and under these conditions, the resonance phenomenon, also known as the Mössbauer effect, can be observed. There are a number of good books and articles available about Mössbauer spectroscopy in general,[1,2] and about the application of ^{57}Fe Mössbauer spectroscopy to biochemistry in particular,[3−7] and therefore, we only summarize the salient features of the method in this article.

^{57}Fe Mössbauer spectroscopy can be used to study the chemical nature of Fe-containing species, because changes in the electronic structure perturb the energies of the nuclear levels via the hyperfine interactions. The hyperfine interactions are typically significantly larger than the line width (and can therefore be resolved) but do not exceed a range of 1000 neV. The energy of the emitted γ-photon can be modulated by applying the Doppler effect to the source; the energy difference is given by eq 1, in which v is the velocity of the source, c is the velocity of light, and E_γ is the energy of the emitted γ-photon

$$\Delta E = (v/c)E_\gamma \qquad (1)$$

Using Doppler velocities of approximately ±12 mm/s, which correspond to approximately ±600 neV (1 mm/s corresponds to 48.1 neV), it is possible to scan the energy range covering the hyperfine interactions of Fe. In a typical ^{57}Fe Mössbauer spectroscopic experiment in transmission mode, the γ-photons are counted as a function of the source velocity.

The simplest type of Mössbauer spectrum is schematically shown in Figure 1C. It is commonly referred to as a "quadrupole doublet" and consists of two peaks. The existence of two distinct transitions stems from the interaction of the nuclear quadrupole moment of the excited state and the electric field gradient (EFG) tensor, which results in the splitting of the excited nuclear state into the $M_I = \pm^1/_2$ and $M_I = \pm^3/_2$ levels in the absence of magnetic interactions (see Figure 1B). The energy difference between the two doublets is called the quadrupole splitting parameter, ΔE_Q (Figure 1B), and corresponds to the separation of the two transitions of the quadrupole doublet (Figure 1C).

The EFG tensor has three principal components, V_{xx}, V_{yy}, and V_{zz}. Because the EFG is traceless, i.e., $\Sigma V_{ii} = 0$, only two parameters are required to characterize this interaction fully. They are V_{zz} and the asymmetry parameter, $\eta = (V_{xx} - V_{yy})/V_{zz}$. The conventional Hamiltonian for this interaction is given in eq 2, in which e represents the proton charge and Q the quadrupole moment of the nuclear excited state ($I = {}^3/_2$), and the solution of this Hamiltonian yields ΔE_Q (eq 3).

$$\hat{H}_Q = \frac{eQV_{zz}}{12}[3\mathbf{I}_z^2 - I(I+1) + \eta(\mathbf{I}_x^2 - \mathbf{I}_y^2)] \qquad (2)$$

$$\Delta E_Q = \frac{eQV_{zz}}{2}\sqrt{1 + \eta^2/3} \qquad (3)$$

The isomer shift, which is given by the average position of the two peaks, provides important clues about the oxidation state, spin state, and coordination environment (type and number of ligands, covalency of Fe−ligand bonds). The isomer shift depends on the electron density at the ^{57}Fe nucleus of the sample, $\rho^A(0)$; the electron density at the ^{57}Fe nucleus of the source, $\rho^S(0)$; and the ^{57}Fe nuclear radii in the ground and excited states, R_g and R_e, respectively (eq 4).

$$\delta \propto (R_e^2 - R_g^2)[\rho^A(0) - \rho^S(0)] \qquad (4)$$

The term $(R_e^2 - R_g^2)$ is negative for ^{57}Fe, and therefore, an increase of the electron density at the nucleus of the absorber results in a decrease of its isomer shift, δ. Although only s electrons have a finite density at the nucleus, d electrons influence the s-electron density by shielding, and consequently, the isomer shift is a sensitive measure of the aforementioned properties of the Fe center. The following general rules are often useful for interpretation of Mössbauer isomer shifts: (1) the isomer shifts of low-spin complexes are less than those of high-spin complexes, (2) the isomer shift increases with increasing coordination number of the Fe site, (3) the isomer shift increases in the series $\delta(Fe^{4+}) < \delta(Fe^{3+}) < \delta(Fe^{2+})$, and (4) the isomer shifts of Fe sites coordinated by soft (sulfur) ligands are less than those of Fe

(1) Greenwood, N. N.; Gibb, T. C. *Mössbauer Spectroscopy*; Chapman & Hall: London, 1971.
(2) Gütlich, P.; Link, R.; Trautwein, A. X. *Mössbauer Spectroscopy and Transition Metal Chemistry*; Springer-Verlag: Berlin, 1978.
(3) Münck, E. In *Physical Methods in Bioinorganic Chemistry*; Que, L., Jr., Ed.; University Science Books: Sausalito, CA, 2000; pp 287−319.
(4) Debrunner, P. G. In *Biological Magnetic Resonance*; Berliner, L. J., Reuben, J., Eds.; Kluwer Academic/Plenum Publishers: New York, 1993; Vol. 13, pp 59−101.
(5) Trautwein, A. X.; Bill, E.; Bominaar, E. L.; Winkler, H. *Structure and Bonding*; Springer: Berlin, 1991; Vol. 78, pp 1−95.
(6) Schünemann, V.; Winkler, H. *Rep. Prog. Phys.* **2000**, *63*, 263−353.
(7) Huynh, B. H.; Kent, T. A. *Adv. Inorg. Biochem.* **1984**, *6*, 163−223.

sites coordinated by hard (N, O) ligands. Detailed insight into the dependence of the isomer shift on the chemical nature of the Fe site has recently emerged from computational studies carried out by Neese[8a] and Münck and co-workers.[9]

More detailed information about the electronic structure of the Fe site can be obtained by Mössbauer spectroscopy when the nucleus is subjected to a magnetic field. In a magnetic field, the nuclear levels of the ground and excited states split because of the nuclear Zeeman effect (Figure 1D; $g_n = 0.181$ for the ground state and $g_n = -0.106$ for the excited state; note that the opposite sign of the nuclear g factors results in reverse order of the M_I levels in the ground and excited states), resulting in a six-line Mössbauer spectrum (Figure 1E). These six transitions satisfy the selection rule of Mössbauer spectroscopy, $\Delta M_I = 0, \pm 1$. The magnitude of the splitting depends on the magnitude of the effective magnetic field at the nucleus, $\mathbf{B}_{\text{eff}}$, and this field is the resultant of the externally applied magnetic field, $\mathbf{B}_{\text{ext}}$, which can be controlled experimentally, and the internal magnetic field, $\mathbf{B}_{\text{int}}$, which is an intrinsic property of a given Fe species. The relative intensity of the six transitions depends on the angle between $\mathbf{B}_{\text{eff}}$ and the propagation direction of the γ-photon (Figure 1E). If $\mathbf{B}_{\text{eff}}$ is perpendicular to the γ-photon, the intensity of the $\Delta M_I = 0$ transitions reaches a maximum, resulting in a 3:4:1:1:4:3 ratio of the six transitions. When $\mathbf{B}_{\text{eff}}$ is parallel to the γ-photon, the $\Delta M_I = 0$ transitions are forbidden, yielding a 3:0:1:1:0:3 ratio. Finally, when $\mathbf{B}_{\text{eff}}$ is orientation-averaged, an intensity ratio of 3:2:1:1:2:3 is observed. $\mathbf{B}_{\text{eff}}$ is often dominated by the size and anisotropy of $\mathbf{B}_{\text{int}}$, which is caused by paramagnetic electronic states of the Fe site. Therefore, the positions and relative intensities of the transitions in a magnetic Mössbauer spectrum provide detailed insight into the electronic structure of the Fe site.

The magnetic properties of a single transition metal ion are commonly described by the following spin Hamiltonian[10]

$$\hat{H}_{\text{el}} = \beta \mathbf{S}\cdot\mathbf{g}\cdot\mathbf{B} + \mathbf{S}\cdot\mathbf{D}\cdot\mathbf{S} \qquad (5)$$

The first term represents the electronic Zeeman effect, which describes the interaction of the spin, **S**, with the magnetic field, **B**. This interaction is described by the **g** tensor, which has three principal components, g_x, g_y, and g_z. With transition metals, these components can deviate substantially from the free electron g value, $g_e = 2.0023$, as a consequence of the coupling between the spin and orbital angular momenta. The second term of eq 5 is known as the zero-field splitting (ZFS) interaction and originates from second-order perturbation treatment of the interaction of spin and orbital angular momenta. For systems with $S \geq 1$, this interaction lifts the $(2S + 1)$-fold degeneracy in the absence of an applied magnetic field. It is typically written in the following form (eq 6)

$$\mathbf{S}\cdot\mathbf{D}\cdot\mathbf{S} = D\left[\mathbf{S}_z^2 - \frac{S(S+1)}{3}\right] + E(\mathbf{S}_x^2 - \mathbf{S}_y^2) \qquad (6)$$

The parameters D and E are the axial and rhombic ZFS parameters, respectively. It is customary to report the ratio E/D, which is also termed "rhombicity". With respect to the effect of ZFS on Mössbauer spectra, there is an important distinction between systems with half-integer-spin and those with integer-spin ground states. The electronic spin states of all half-integer-spin species are split into $(S + {}^1/_2)$ Kramers doublets, and the 2-fold degeneracy remains in zero field, regardless of the ZFS parameters D and E. In contrast, the degeneracy of the $(2S + 1)$ levels is removed for integer-spin systems for $E/D \neq 0$. To illustrate the effect of the Zeeman and ZFS interaction, we show the energies (top row) and the spin expectation values $\langle S \rangle$ (bottom row) of an $S = {}^5/_2$ system (Figure 2A) and an $S = 2$ system (Figure 2B) as a function of the magnetic field. The first column shows the effect of the Zeeman splitting alone, i.e., no ZFS. The second and third columns have been calculated for the axial case ($E/D = 0$) with $D = +10\ \text{cm}^{-1}$ and B oriented along the x-axis and z-axis, respectively. The last three columns represent the fully rhombic case ($E/D = 1/3$) calculated for $D = +10\ \text{cm}^{-1}$ and with B oriented along the x-, y-, and z-axes, respectively. $\langle S \rangle$ is calculated from the eigenvectors of the solution of eq 5 for each of the $(2S + 1)$ states. In zero magnetic field, each of the three Kramers doublets of an $S = {}^5/_2$ system has at least one orientation exhibiting a significant value of $\langle S \rangle$, whereas the $S = 2$ system exhibits $\langle S \rangle$ values of zero in the absence of a magnetic field (except for the singular point with $E/D = 0$ and **B** oriented along the z axis).

As a result of the behavior illustrated in Figure 2, half-integer-spin systems give rise to large $\langle S \rangle$ values for $\mathbf{B}_{\text{ext}} = 40$ mT, of up to $|\langle S \rangle| \approx 2.5$ for high-spin Fe(III). This has an important consequence for spectra recorded in small magnetic fields ($\sim$40 mT), because the internal magnetic field is directly proportional to $\langle S \rangle$ (eq 7).

$$\mathbf{B}_{\text{int}} = -\langle \mathbf{S} \rangle \cdot \mathbf{A}/g_n\beta_n \qquad (7)$$

The **A** tensor for ^{57}Fe is dominated by the Fermi contact term, which typically has a value of $A/g_n\beta_n \approx -20$ to -22 T and yields internal magnetic fields of $\sim$50 T. Therefore, half-integer-spin systems yield magnetically split spectra if the relaxation of the electronic spin is slow (vide infra). For the electronic ground state, the internal magnetic field is oriented antiparallel to the external magnetic field. Because the absolute magnitude of $\mathbf{B}_{\text{int}}$ is larger than that of $\mathbf{B}_{\text{ext}}$, it follows that $\mathbf{B}_{\text{eff}}$ *decreases* with *increasing* $\mathbf{B}_{\text{ext}}$ for an Fe site exhibiting its saturation spin expectation value.

In most cases, integer-spin systems exhibit spin expectation values of almost zero in a 40-mT magnetic field and thus yield quadrupole doublets, but there are exceptions: For certain combinations of ZFS parameters, a species with an integer-spin ground state (in particular, one with large value of S) can have a significant spin expectation value, giving rise to magnetically split spectra. For example, Münck and

(8) (a) Neese, F. *Inorg. Chim. Acta* **2002**, *337*, 181−192. (b) Neese, F. *Curr. Opin. Chem. Biol.* **2003**, *7*, 125−135.
(9) Vrajmasu, V.; Münck, E.; Bominaar, E. L. *Inorg. Chem.* **2003**, *42*, 5974−5988.
(10) Abragam, A.; Bleaney, B. *Electron Paramagnetic Resonance of Transition Metal Ions*; Dover: New York, 1986.

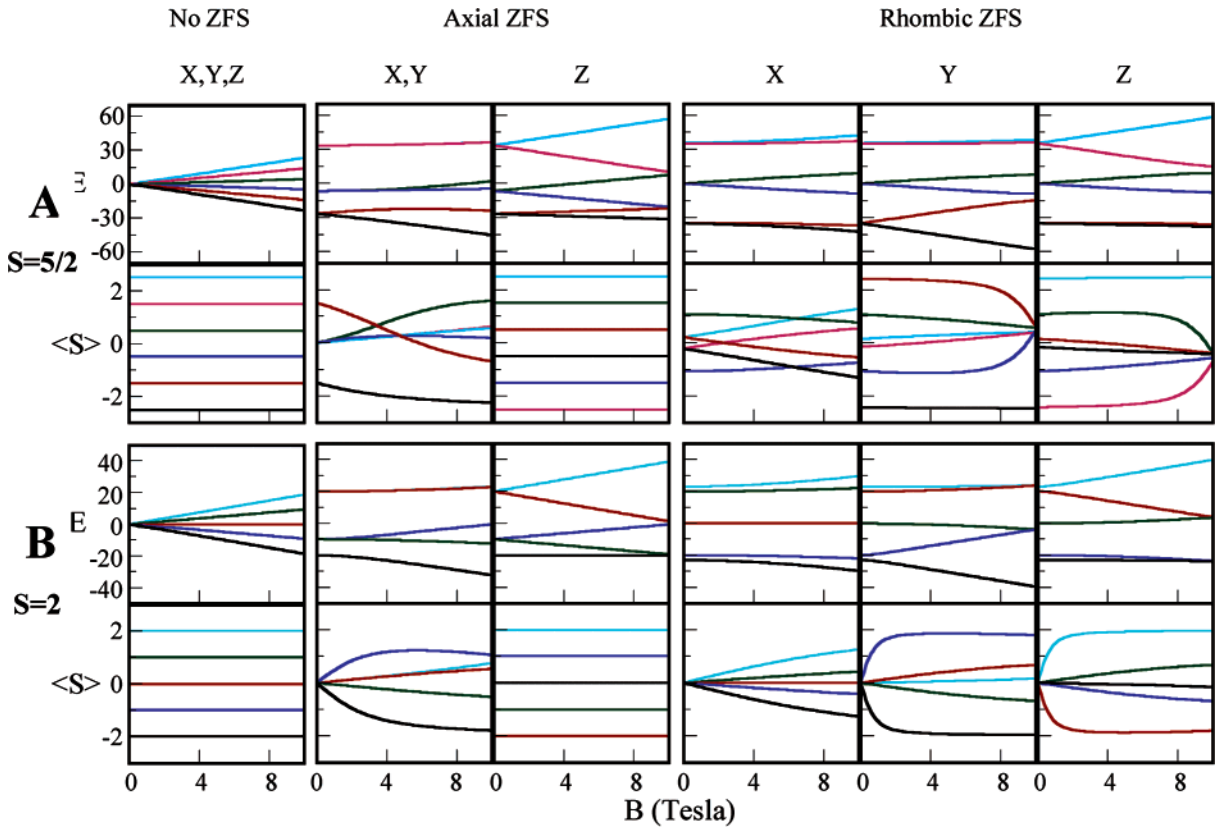

Figure 2. Energies (top) and spin expectation values (bottom) of (A) an $S = {}^5/_2$ system and (B) an $S = 2$ system. The calculations were carried out by using the following parameters: $D = 0$ cm^{-1} (column 1); $D = 10$ cm^{-1}, $E/D = 0$ (columns 2 and 3); $D = 10$ cm^{-1}, $E/D = {}^1/_3$ (columns 4−6). The orientation of the magnetic field is indicated on top of each column.

co-workers demonstrated that the "all-ferrous" $[4Fe-4S]^0$ cluster has an $S = 4$ ground state and exhibits magnetically split spectra.[11]

Another important aspect of electronic structure is the interaction between two or more paramagnetic centers.[12] Two different interactions can be observed. The first arises from orbital overlap and electrostatic interactions between two paramagnetic centers, either directly between the two centers (e.g., a metal center and a coordinated radical) or mediated by one or more bridging atoms. The second interaction is through-space magnetic−dipolar coupling. The first interaction is usually 2−3 orders of magnitude stronger than the second and dominates in polynuclear transition metal complexes containing bridging ligands.

Coupling between two paramagnetic centers having spins $\mathbf{S}_1$ and $\mathbf{S}_2$ yields states with total spin $\mathbf{S}$, which can have values $|S_1 - S_2|$, $|S_1 - S_2 + 1|$, ..., $S_1 + S_2$. The relative energies of the different total spin states can be calculated using the phenomenological Heisenberg−Dirac−van Vleck Hamiltonian, eq 8, in which J is the isotropic exchange coupling constant. The solutions of this Hamiltonian are given by eq 9.

$$\hat{H}_{\text{exchange}} = J\mathbf{S}_1\cdot\mathbf{S}_2 \tag{8}$$

$$E(S) = (J/2)S(S+1) \tag{9}$$

In this definition, positive J values correspond to antiferromagnetic coupling between the two paramagnetic centers resulting in an $S = |S_1 - S_2|$ ground state, and conversely, negative values describe a ferromagnetic interaction yielding an $S = S_1 + S_2$ ground state. For the case $|J| > |D_i|$, $i = 1$, 2, the g and D values for each of the total spin states, g_S and D_S, can be expressed in terms of the local D_i and g_i values using standard spin projection techniques,[12−15] as shown in the following equations

$$D_S = \sum_{i=1,2} d_{i,S}D_i \qquad \text{and } g_S = \sum_{i=1,2} c_{i,S}g_i \tag{10}$$

The spin-coupling coefficients $c_{i,S}$ are defined as follows (S_j denotes the other spin)

$$c_{i,S} = \frac{S(S+1) + S_i(S_i+1) - S_j(S_j+1)}{2S(S+1)} \tag{11}$$

A few important features of the Mössbauer and EPR spectra of exchange-coupled Fe-containing clusters can be illustrated by considering an antiferromagnetically coupled dinuclear cluster with $S_1 = {}^5/_2$ and $S_2 = 2$. Examples of such species found in biological systems include the $[2Fe-2S]^+$ clusters, Fe(II)/Fe(III) states of non-heme diiron proteins, and the Fe(III)/Fe(IV) cluster **X** from ribonucleotide reductase.

(11) Yoo, S. J.; Angove, H. C.; Burgess, B. K.; Hendrich, M. P.; Münck, E. *J. Am. Chem. Soc.* **1999**, *121*, 2534−2545.
(12) Kahn, O. *Molecular Magnetism*; VCH: New York, 1993.
(13) Gibson, J. F.; Hall, D. O.; Thornley, J. H. M.; Whatley, F. R. *Proc. Natl. Acad. Sci. U.S.A.* **1966**, *56*, 987−990.
(14) Scaringe, R. P.; Hodgson, D. J.; Hatfield, W. E. *Mol. Phys.* **1978**, *35*, 701−713.
(15) Bencini, A.; Gatteschi, D. *EPR of Exchange Coupled Systems*; Springer-Verlag: Berlin, 1990.

Under the assumption $J > |D_i|$, $i = 1, 2$, the $S = {}^1/_2$ ground state is well isolated. EPR spectroscopy senses the total spin of the system, $S = {}^1/_2$, and allows determination of the three principal components of the **g** tensor. The Mössbauer spectra exhibit two subspectra of equal intensity, corresponding to the two distinct Fe sites of the dinuclear cluster. The internal magnetic field at each of the two Fe sites depends on the projection of each intrinsic spin onto the total spin *S*. The projection factors are also given by eq 11 and yield values of $c_{1,1/2} = {}^7/_3$ and $c_{2,1/2} = -{}^4/_3$ for the $S = {}^1/_2$ ground state of our example. The different signs of the $c_{i,S}$ values have an important consequence for the field dependence of the two subspectra: the first Fe site ($S_1 = {}^5/_2$) exhibits the normal field dependence (i.e., for the electronic ground state, $\mathbf{B}_{\text{eff}}$ *decreases* with *increasing* $\mathbf{B}_{\text{ext}}$), whereas the second Fe site exhibits the opposite behavior (i.e., for the electronic ground state, $\mathbf{B}_{\text{eff}}$ *increases* with *increasing* $\mathbf{B}_{\text{ext}}$). Consequently, analysis of the field dependence of $\mathbf{B}_{\text{int}}$ in the Mössbauer spectra provides important insight into the exchange interaction(s) of an Fe-containing cluster with a paramagnetic ground state. This effect is illustrated in Figure 3A for the Fe(III)/Fe(IV) cluster **X** from ribonucleotide reductase.

For the computation of Mössbauer spectra, the Hamiltonian shown in eq 12 is used, in which the first term includes the electron Zeeman and ZFS interactions (eq 5); the second term represents the hyperfine interaction between the spin and the ^{57}Fe nucleus, $\mathbf{S}\cdot\mathbf{A}\cdot\mathbf{I}$; and the third term contains the nuclear Zeeman interaction, $-\beta_n g_n \mathbf{I}\cdot\mathbf{B}$, and the quadrupole interaction of the excited nuclear state (eq 2).

$$\hat{H} = \hat{H}_{\text{el}} + \hat{H}_{\text{hf}} + \hat{H}_{\text{nuc}} \tag{12}$$

In the presence of a small externally applied magnetic field, $\mathbf{B}_{\text{ext}} \geq 10$ mT, the first term of eq 12 dominates, and it is possible to separate it from the rest of the Hamiltonian. Then, the spin expectation value, $\langle\mathbf{S}\rangle$, is calculated for each electronic state and these values are substituted for **S** in the hyperfine coupling term (eq 13).

$$\hat{H} = \langle\mathbf{S}\rangle\cdot\mathbf{A}\cdot\mathbf{I} - \beta_n g_n \mathbf{I}\cdot\mathbf{B} + \hat{H}_{\text{Q}} \tag{13}$$

For the computation of the Mössbauer spectrum, the rate of electronic spin fluctuation in comparison with the precession rate of the ^{57}Fe nucleus is crucial. If the electronic spin fluctuates more slowly than the ^{57}Fe Larmor frequency, then each electronic state gives rise to its own Mössbauer spectrum, and the resulting Mössbauer spectrum is the superposition of the spectra of all individual electronic states, weighted according to their Boltzmann population factors. If the fluctuation of the electronic spin is fast in comparison with the ^{57}Fe Larmor frequency, the nucleus will sense the Boltzmann-population-weighted average of the spin expectation values of all thermally populated states, $\langle\mathbf{S}\rangle_{\text{av}}$, and the Mössbauer spectrum can be calculated using eq 13 with $\langle\mathbf{S}\rangle = \langle\mathbf{S}\rangle_{\text{av}}$. If the fluctuation rate of the electronic spin is comparable to the ^{57}Fe Larmor frequency, the analysis is significantly more complicated.[6,16] To avoid these complexities, one tries to choose experimental conditions that satisfy either of the two limiting cases. At 4.2 K, most Fe-containing proteins give rise to Mössbauer spectra characteristic of the slow relaxation limit. The final step in the calculation of a Mössbauer spectrum is to shift the entire calculated spectrum by δ, the isomer shift.

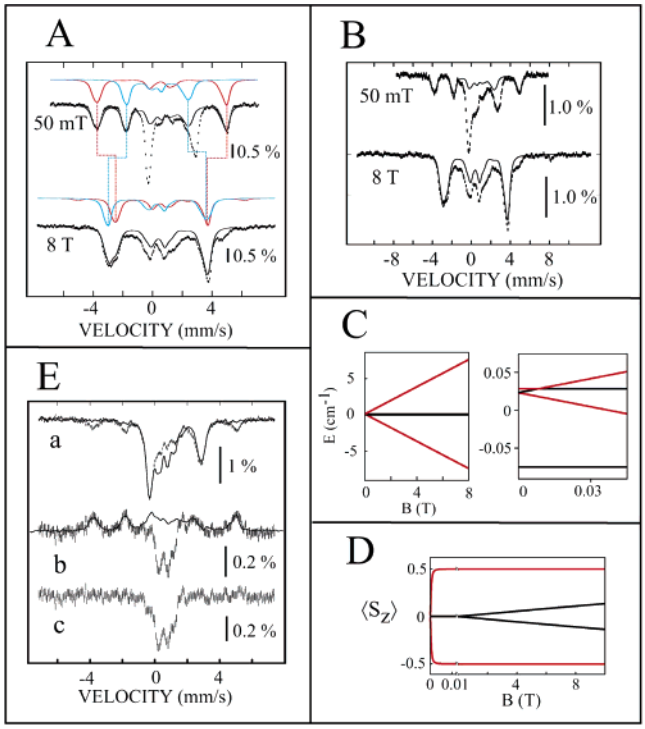

Figure 3. (A) Mössbauer spectra of a 310-ms RFQ sample from the reaction of Fe(II), apo R2−Y122F, and O_2. The spectra were recorded at 4.2 K in (a) 50-mT and (b) 8-T external magnetic fields and are adapted from Ravi et al.[39] A simulation of the spectrum of **X** according to parameters reported by Sturgeon et al.[49] (see Table 1) is shown in black and corresponds to 70% of the total intensity. The individual contributions of the Fe(III) and Fe(IV) sites are shown in red and blue. The field dependence of these components is indicated by dotted lines. (B) Spectra of a 19-ms sample of the reaction of wild-type Fe(II)-R2 with O_2 recorded at 4.2 K in (a) 50-mT and (b) 8-T external magnetic fields. The contribution of normal **X** is shown as a solid line and corresponds to 47% and 67% of the total intensity, respectively. The spectra are adapted from Baldwin et al.[54] (C) Energies and (D) spin expectation values of the four states of the diradical system, adapted from Krebs et al.[55] (E) Resolution of the Mössbauer spectrum of a $(Fe_2O_2)^{4+}$ precursor to cluster **X**: (a) spectra of RFQ samples prepared by mixing the Fe(II)-R2-W48A/Y122F complex with O_2, incubating to allow for accumulation of the precursor to **X**, and then mixing either with 3-methylindole to trigger conversion of the precursor to **X** (hashed) or with buffer as a control (solid); (b) difference spectrum from two spectra in a (hashed) and features emanating from **X** and the product diiron(III) cluster that form after the mix with 3-methylindole (solid); (c) spectrum of the $(Fe_2O_2)^{4+}$ precursor of **X** obtained after removal of the solid line in b from the difference spectrum. All spectra are adapted from Saleh et al.[93]

If the Fe site for which the Mössbauer spectrum is calculated is part of an exchange-coupled cluster (e.g., a dinuclear cluster), the electron Zeeman and ZFS interactions of the second spin (eq 5) and the interaction between the two spins (eq 8) need to be added to the electronic Hamiltonian, and the computation is carried out as described before. When the electron spin ground state of the cluster, *S*, is well separated from excited spin states (i.e., when the exchange coupling constant *J* is large), it is possible to simplify the calculation of the spin expectation values to be used in eq 13 by considering only the spin ground state. In

(16) Schulz, C. E.; Nyman, P.; Debrunner, P. G. *J. Chem. Phys.* **1987**, *87*, 5077−5091.

this case, g_S and D_S of the total spin ground state have to be calculated from the local g_i and D_i values using eq 10. Similarly, the A values in eq 13 need to be multiplied by the appropriate spin-projection factor, $c_{i,S}$. It is important to keep in mind that the latter procedure yields accurate results only if the spin ground state is sufficiently well separated from excited spin states.

Calculation of Mössbauer Parameters Using Density Functional Methods

A particularly important development in the field has been the ability to accurately calculate Mössbauer parameters using density functional methods. Recent reports have shown that, on average, quadrupole splittings, ΔE_Q, can be obtained to within 0.30 mm/s,[17] but errors of 0.30−0.50 mm/s are not uncommon.[8b] Isomer shifts, δ, can be predicted to within 0.10 mm/s.[8a,17] These results are exciting: they suggest that a combination of computation and Mössbauer spectroscopy can yield structural information about reactive enzymatic intermediates.

Quadrupole splittings are determined by the electric field gradient (EFG) at the iron nucleus (eq 3). The EFG can be calculated with virtually any standard quantum chemistry program. Given the gradient, one needs only Q, the quadrupole moment of the $I = {}^3/_2$ excited state of the ^{57}Fe nucleus, to obtain the splitting. Dufek and co-workers determined what is believed to be the most accurate value of Q (1.6 barn), by comparing experimental quadrupole splittings with calculated EFGs for a number of Fe compounds.[18] Using this value, Oldfield was able to calculate quadrupole splittings for 23 molecules (covering a range of 5.63 mm/s) with a root-mean-square deviation (RMSD) of 0.31 mm/s. Excellent results were obtained with both pure (BPW91) and hybrid (B3LYP) functionals, using a Wachters basis set (62111111/3311111/311) on Fe, a 6-311G* basis set on all other heavy atoms, and a 6-31G* basis set on H.

The theoretical determination of isomer shifts requires knowledge of the electron density at the nucleus, $\rho^A(0)$. This quantity is the only variable in the expression for the isomer shift. As a result, eq 4 can be rewritten as

$$\delta = a[\rho^A(0) - c] \tag{14}$$

Using this equation, one can determine the constants a and c for a given basis set and functional through a comparison of the calculated $\rho^A(0)$ values and the experimentally determined isomer shifts for a series of molecules. Both Neese and Oldfield have provided parametrizations for this linear equation. Using pure and hybrid functionals, they examined a number of compounds (spanning six spin states and five oxidation states) and found excellent agreement between theory and experiment with an RMSD of ∼0.10 mm/s over a range of ∼2.3 mm/s. *It is important to remember that each parametrization of eq 14 is applicable only to the basis set and functional with which it was determined.* Oldfield parametrized eq 14 using the Wachters, 6-311G*, and 6-31G* basis sets as described above. Neese has shown that minor distortions in the inner-shell orbitals can lead to comparatively large fluctuations in the value of $\rho^A(0)$, and he has developed a core-properties (CP) basis set with increased flexibility in the core region to deal with this issue. His parametrization of eq 14 uses this CP basis.

Mössbauer Spectroscopy in Bioinorganic Chemistry

Iron is the most structurally and functionally diverse transition metal in biological systems, and because Mössbauer spectroscopy can provide detailed insight into the chemical nature of the iron site, the technique has played a key role in the biophysical characterization of Fe-containing proteins. Three groups of proteins, containing either (1) heme iron, (2) Fe/S clusters, or (3) non-heme, non-Fe/S iron, have been studied extensively. Work on the heme proteins has been summarized by Debrunner, and we refer the reader to this review article.[19] For the Fe/S proteins, Mössbauer spectroscopy played a pivotal role, especially in the determination of the electronic structures of the various cluster forms.[7,20−23] In the study of the non-heme iron enzymes, Mössbauer spectroscopy provided unique insight into the reaction mechanisms and allowed for determination of how the enzymes control the reactivity of their Fe centers. In these studies, samples suitable for Mössbauer spectroscopy were prepared by the rapid freeze-quench (RFQ) method. This approach allows one to monitor changes on the millisecond time scale at the Fe site participating in a biochemical reaction. In the following section, we introduce this method and summarize its applications.

RFQ Mössbauer Spectroscopy and Reaction Intermediates. In the RFQ method, a reaction is initiated by rapid mixing and is allowed to proceed for a defined reaction time as it flows through an "aging hose" of appropriate length/volume. Upon emerging from this hose, the solution is sprayed into a cold cryosolvent. The resulting rapid freezing stops the reaction and produces snow-like particles that can be collected into a spectroscopy cell. With the reactant-mixing and -flow systems that have traditionally been employed, "quench times" (the time between injection of the solution into the cryosolvent and cessation of the reaction) of 5−10 ms have generally been estimated, but recent advances have afforded much shorter quench times.[24−26] Equipment originally developed for the collection of the frozen particles into tubes suitable for electron paramagnetic

(17) Zhang, Y.; Mao, J.; Godbout, N.; Oldfield, E. *J. Am. Chem. Soc.* **2002**, *124*, 13921−13930.
(18) Dufek, P.; Blaha, P.; Schwarz, K. *Phys. Rev. Lett.* **1995**, *75*, 3545−3548.
(19) Debrunner, P. G. *Phys. Bioinorg. Chem. Ser.* **1989**, *4*, 137−234.
(20) Münck, E.; Kent, T. A. *Hyperfine Interact.* **1986**, *27*, 161−172.
(21) Münck, E.; Papaefthymiou, V.; Surerus, K. K.; Girerd, J.-J. *ACS Symp. Ser.* **1988**, *372*, 302−325.
(22) Girerd, J.-J.; Papaefthymiou, V.; Surerus, K. K.; Münck, E. *Pure Appl. Chem.* **1989**, *61*, 805−816.
(23) Beinert, H.; Holm, R. H.; Münck, E. *Science* **1997**, *277*, 653−659.
(24) Tanaka, M.; Matsuura, K.; Yoshioka, S.; Takahashi, S.; Ishimori, K.; Hori, H.; Morishima, I. *Biophys. J.* **2003**, *84*, 1998−2004.
(25) Lin, Y.; Gerfen, G. J.; Rousseau, D. L.; Yeh, S.-R. *Anal. Chem.* **2003**, *75*, 5381−5386.
(26) Cherepanov, A. V.; de Vries, S. *Biochim. Biophys. Acta* **2004**, *1656*, 1−31.

resonance (EPR) spectroscopy[27,28] was subsequently adapted for the preparation of samples for Mössbauer[29,30] and X-ray absorption spectroscopies,[31−35] and more recent developments have permitted application of RFQ to an even wider variety of spectroscopic techniques. Use of liquid ethane as the cryogen allows for removal by evaporation, permitting application to spectroscopies for which cryo-solvent interference might otherwise be prohibitive (e.g., resonance Raman).[36] Injection directly into liquid nitrogen followed by cryogenic mulling of the frozen sample in ethylene glycol has been used to generate optical-quality glasses for circular dichroism (CD) and magnetic circular dichroism (MCD) spectroscopies.[37] A liability of this approach is that the quench time can be as much as 10 times longer for liquid-nitrogen quenching. An additional complication is that the intermediate might decay during the mulling/sample-transfer procedure. In application of these alternative quenching and spectroscopic methods, it is generally true that an intermediate that has already been detected (often by RFQ Mössbauer spectroscopy) is being targeted for further characterization. By allowing for facile assessment of the prevalence (purity) of the target species before and after physical manipulation (e.g., cryogenic mulling) or spectroscopic experiments (e.g., irradiation during X-ray experiments), Mössbauer spectroscopy can serve important accessory and quality-control functions.

RFQ Mössbauer spectroscopy has become an important technique in mechanistic studies of iron proteins, particularly because of its unique capability to detect all iron-containing species, regardless of their chemical nature (provided that they contain ^{57}Fe; vide infra). RFQ samples are necessarily heterogeneous, comprising reactants, accumulating intermediates, and products, in proportions dictated by the reaction time and the inherent kinetic characteristics of the reaction. Therefore, the Mössbauer spectrum of an RFQ sample will represent the superposition of subspectra of these various components. The relative contribution of each subspectrum (the fraction of the total absorption area that it contributes to the experimental spectrum) is proportional to the concentration of the corresponding Fe species, based on the justified assumption that the recoilless fraction at 4.2 K is the same for each Fe species. Thus, analysis of RFQ Mössbauer spectra generally involves deconvolution of the experimental spectrum into appropriately weighted theoretical or experimental reference spectra. If the subspectra are well-resolved, the analysis is straightforward. In this case, the relative contribution of each Fe species and (often) Mössbauer parameters of previously unknown (intermediate) species can be determined accurately. However, if the subspectra overlap significantly, the deconvolution analysis is time-consuming and complex, and Mössbauer parameters and relative areas have significantly larger uncertainties. In such a situation, it might be possible to simplify the deconvolution by recording Mössbauer spectra at different temperatures or different externally applied fields, with the intent to enhance resolution of the subspectra.

RFQ EPR spectroscopy can often complement RFQ Mössbauer spectroscopy in the identification and characterization of Fe-containing reaction intermediates. Species with half-integer-spin ground states are generally EPR-active, and the parameters describing the electronic spin (ZFS parameters and principal components of the **g** tensor) can be determined with great accuracy by EPR spectroscopy in many cases. These parameters can then be used for the simulation of the complex, magnetically split Mössbauer spectra. In addition, integration of EPR resonances can provide quantitation of half-integer-spin species, which are more challenging to quantify by Mössbauer spectroscopy because of the increased complexity associated with magnetically split spectra. On the other hand, species with integer-spin ground states are (in general) not EPR-active. Because these species generally have small values of $\langle S \rangle$, they often give rise to Mössbauer quadrupole doublets, allowing for small amounts ($\sim$5−10% of the total absorption intensity) to be detected, if the new features are sufficiently well resolved. Therefore, the combination of the two methods provides both a detailed picture of the electronic structure of an Fe-containing species and a high probability that it can be quantified.

As discussed above, RFQ Mössbauer spectroscopy—often in conjunction with RFQ EPR spectroscopy—can potentially yield (1) kinetics for each iron complex that accumulates in a reaction and (2) important insight into the chemical nature of each species that accumulates. However, sample requirements for Mössbauer spectroscopy (concentrations of $\gtrsim$1 mM of the Mössbauer-active isotope, ^{57}Fe, which has a natural abundance of only 2.2%; a sample volume of 300−400 μL; $\sim$8 or more samples required to define the kinetics of a biochemical reaction) prevented the full potential of RFQ Mössbauer spectroscopy as a kinetic and mechanistic tool from being fully exploited until the late 1980s. Great strides in molecular biology, which made possible the expression of many proteins in heterologous hosts (e.g., *Escherichia coli*) that are amenable to growth in media enriched with ^{57}Fe, made it more routinely feasible to obtain the large quantities of ^{57}Fe-enriched iron proteins required by the method and paved the way for the pioneering RFQ Mössbauer experiments of Huynh and co-workers in the early 1990s.[38−41]

(27) Bray, R. C. In *Rapid Mixing and Sampling Techniques in Biochemistry*; Chance, B., Eisenhart, R. H., Gibson, Q. H., Lonberg-Holm, K. K., Eds.; Academic Press: New York, 1964; p 195.
(28) Ballou, D. P.; Palmer, G. A. *Anal. Chem.* **1974**, *46*, 1248−1253.
(29) Rutter, R.; Hager, L. P.; Dhonau, H.; Hendrich, M. P.; Valentine, M.; Debrunner, P. G. *Biochemistry* **1984**, *23*, 6809−6816.
(30) Bollinger, J. M., Jr.; Tong, W. H.; Ravi, N.; Huynh, B. H.; Edmondson, D. E.; Stubbe, J. *Methods Enzymol.* **1995**, *258*, 278−303.
(31) Shu, L.; Nesheim, J. C.; Kauffmann, K. E.; Münck, E.; Lipscomb, J. D.; Que, L., Jr. *Science* **1997**, *275*, 515−518.
(32) Riggs-Gelasco, P. J.; Shu, L.; Chen, S.; Burdi, D.; Huynh, B. H.; Que, L., Jr.; Stubbe, J. *J. Am. Chem. Soc.* **1998**, *120*, 849−860.
(33) Riggs-Gelasco, P. J.; Price, J. C.; Guyer, R. B.; Brehm, J. H.; Barr, E. W.; Bollinger, J. M., Jr.; Krebs, C. *J. Am. Chem. Soc.* **2004**, *126*, 8108−8109.
(34) Hwang, J.; Krebs, C.; Huynh, B. H.; Edmondson, D. E.; Theil, E. C.; Penner-Hahn, J. E. *Science* **2000**, *287*, 122−125.
(35) Baldwin, J.; Krebs, C.; Saleh, L.; Stelling, M.; Huynh, B. H.; Bollinger, J. M., Jr.; Riggs-Gelasco, P. J. *Biochemistry* **2003**, *42*, 13269−13279.
(36) Moënne-Loccoz, P.; Krebs, C.; Herlihy, K.; Edmondson, D. E.; Theil, E. C.; Huynh, B. H.; Loehr, T. M. *Biochemistry* **1999**, *38*, 5290−5295.
(37) Mitic, N.; Saleh, L.; Schenk, G.; Bollinger, J. M., Jr.; Solomon, E. I. *J. Am. Chem. Soc.* **2003**, *125*, 11200−11201.

Scheme 1. Reactions (Left Panel) and Reaction Intermediates (Right Panel) of Diiron Carboxylate Proteins

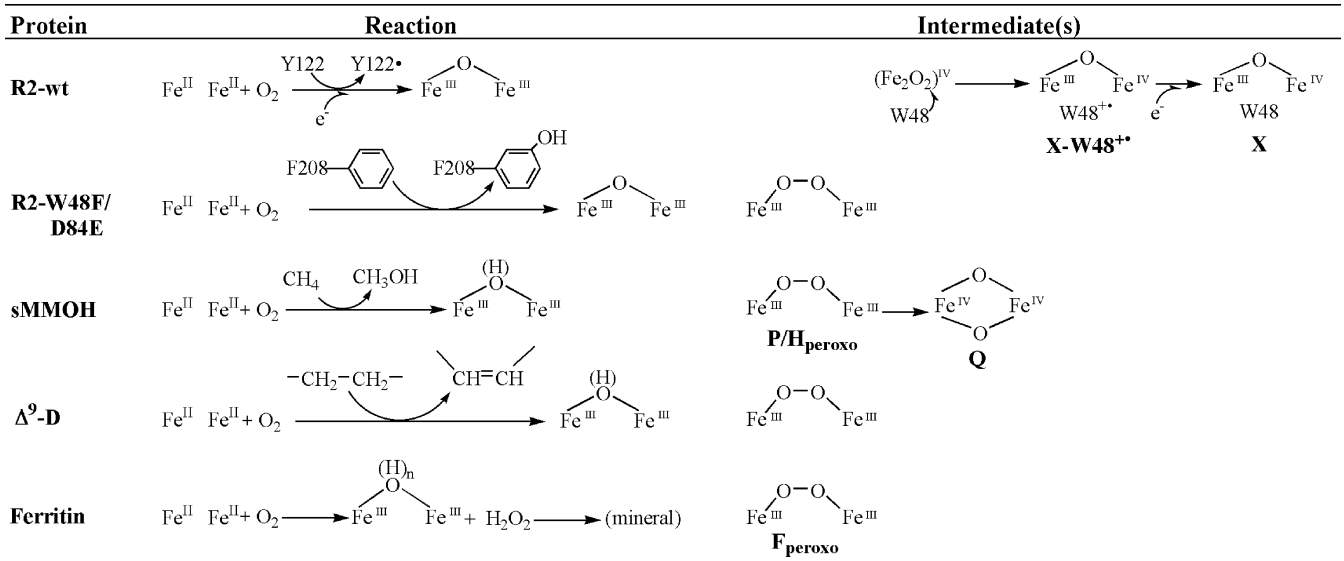

The first successful marriage of the RFQ method and Mössbauer spectroscopy was reported by Debrunner and co-workers, who trapped and characterized the compound I intermediate in the fungal heme iron enzyme, chloroperoxidase (CPO).[29] Whereas this seminal study showed the potential of RFQ Mössbauer spectroscopy as a tool for characterization of iron intermediates, the large rate constants for the CPO catalytic cycle precluded the most auspicious use of the technique: *monitoring the kinetics of a single turnover*. The first hint of the application of RFQ Mössbauer spectroscopy as a true transient-state kinetic method was provided by Beinert, Münck, and co-workers in a study on the enzyme aconitase, which catalyzes dehydration of citrate to *cis*-aconitate and hydration of *cis*-aconitate to isocitrate at the unique (not cysteine coordinated) Fe_a site of a [4Fe−4S] cluster.[42] The authors used the method to measure the kinetics of binding of substrate, intermediate, and product to the enzyme.

Oxygen Activation by the Non-heme Diiron Carboxylate Enzymes. The first time the potential of RFQ Mössbauer spectroscopy as a kinetic method was fully exploited was in the study of assembly of the essential metallocofactor in *Escherichia coli* ribonucleotide reductase.[38,39,43−45] Reichard and co-workers had previously shown that this cofactor, a (μ-oxo)diiron(III) cluster adjacent to a tyrosyl free radical formed by one-electron oxidation of residue 122 (Y122), assembles spontaneously from Fe(II), O_2, and the R2 apo protein (Scheme 1).[46] The protein first binds Fe(II) ions to form a diiron(II) cluster, and this cluster then activates O_2 to carry out Y122 oxidation with concomitant production of the (μ-oxo)diiron(III) cluster. The reaction stoichiometry is interesting, in that O_2 is reduced by four electrons to the oxidation state of two water molecules, whereas only three electrons are provided by oxidation of Y122 and the diiron(II) center. Several studies showed that a third Fe(II) can be oxidized to provide this "extra" electron and that reductants such as ascorbate can also provide it.[44,47,48] Upon mixing of O_2-saturated solutions of apo R2 and Fe(II), two different intermediate states were detected.[43] The first, which exhibits a broad absorption feature at 560 nm, accumulates only when sources of the extra electron are not present [i.e., when Fe(II) is limiting and other reductants are omitted]. Its identity will be discussed below. The second, which has come to be known as cluster **X**, exhibits a broad absorption band at ∼360 nm and a sharp, nearly isotropic, $g = 2.0$ EPR singlet.[43] Hyperfine splitting of its EPR singlet by ^{57}Fe indicated that this species is iron-based, paving the way for its characterization by RFQ Mössbauer spectroscopy.[38] The Mössbauer spectrum of **X** and its dependence on applied magnetic field showed two resolved Fe sites with electronic hyperfine coupling of opposite sign and different magnitude (see Figure 3A and Table 1). One site has a nearly isotropic **A** tensor and parameters squarely in the range for high-spin Fe(III) ions with N/O ligation. Extraction of the parameters of the second site required insight from ^{57}Fe ENDOR experiments, which defined its **A** tensor.[49] The Mössbauer, EPR, and ENDOR data together indicate that the second site has an

(38) Bollinger, J. M., Jr.; Stubbe, J.; Huynh, B. H.; Edmondson, D. E. *J. Am. Chem. Soc.* **1991**, *113*, 6289−6291.
(39) Ravi, N.; Bollinger, J. M., Jr.; Huynh, B. H.; Edmondson, D. E.; Stubbe, J. *J. Am. Chem. Soc.* **1994**, *116*, 8007−8014.
(40) Liu, K. E.; Wang, D.; Huynh, B. H.; Edmondson, D. E.; Salifoglou, A.; Lippard, S. J. *J. Am. Chem. Soc.* **1994**, *116*, 7465−7466.
(41) Liu, K. E.; Valentine, A. M.; Wang, D.; Huynh, B. H.; Edmondson, D. E.; Salifoglou, A.; Lippard, S. J. *J. Am. Chem. Soc.* **1995**, *117*, 10174−10185.
(42) Kent, T. A.; Emptage, M. H.; Merkle, H.; Kennedy, M. C.; Beinert, H.; Münck, E. *J. Biol. Chem.* **1985**, *260*, 6871−6881.
(43) Bollinger, J. M., Jr.; Edmondson, D. E.; Huynh, B. H.; Filley, J.; Norton, J. R.; Stubbe, J. *Science* **1991**, *253*, 292−298.
(44) Bollinger, J. M., Jr.; Tong, W. H.; Ravi, N.; Huynh, B. H.; Edmondson, D. E.; Stubbe, J. *J. Am. Chem. Soc.* **1994**, *116*, 8015−8023.
(45) Bollinger, J. M., Jr.; Tong, W. H.; Ravi, N.; Huynh, B. H.; Edmondson, D. E.; Stubbe, J. *J. Am. Chem. Soc.* **1994**, *116*, 8024−8032.
(46) Atkin, C. L.; Thelander, L.; Reichard, P. *J. Biol. Chem.* **1973**, *248*, 7464−7472.
(47) Elgren, T. E.; Lynch, J. B.; Juarez-Garcia, C.; Münck, E.; Sjöberg, B.-M.; Que, L., Jr. *J. Biol. Chem.* **1991**, *266*, 19265−19268.
(48) Ochiai, E.; Mann, G. J.; Gräslund, A.; Thelander, L. *J. Biol. Chem.* **1990**, *265*, 15758−15761.

Table 1. Mössbauer Parameters of Cluster **X** and Related Valence-Localized Fe(III)/Fe(IV) Compounds with $S = {}^1/_2$ Ground State

species		δ (mm/s)	ΔE_Q (mm/s)	η	$\mathbf{A}/g_n\beta_n$ (T)[a]	ref
X	Fe(III)	0.56	−0.9	0.5	(−53.9, −52.4, −53.2)	49
	Fe(IV)	0.26	−0.6	2.7	(20.0, 26.8, 26.8)	
$\mathbf{Q}_X$ [b]	Fe(III)	0.48	−0.9	0.2	(−50.8, − 54.5, −54.5)	67
	Fe(IV)	0.14	−0.6	0.9	(18.9, 21.8, 21.8)	
Lippard's model compound[c]	Fe(III)	0.56	0.9	−0.3	(−54.5, −51.2, −54.5)	119
	Fe(IV)	0.19	0.8	−1	(18.9, 27.2, 17.3)	
Que's model compound[d]	Fe(III)	0.48	1.6	1.0	(−46.9, −46.9, −46.9)	120
	Fe(IV)	0.08	0.5	1.0	(14.5, 26.5, 26.5)	

[a] Given with respect to the total spin of the ground state, $S = {}^1/_2$. [b] Obtained by cryoreduction of intermediate **Q** of *Methylococcus capsulatus* (Bath) methane monooxygenase. [c] Obtained by oxygenation at −78 °C of $[Fe_2(\mu\text{-}OOCAr^{Tol})_4(4\text{-}^t\text{Bu-pyridine})_2]$, with $OOCAr^{Tol}$ = 2,6-di(*p*-tolyl)-benzoate. [d] $[Fe_2(\mu\text{-}O)_2(6\text{-Me-TPA})_2]^{3+}$, with 6-Me-TPA = *N*-(6-methyl-2-pyridylmethyl)-*N*,*N*-bis(2-pyridylmethyl)-amine.

oxidation state between 3+ and 4+, leading to a simplest formulation of **X** as an ($S = {}^1/_2$) Fe(III)/Fe(IV) complex with significant delocalization of spin density from the Fe(IV) site onto its ligands.[49] Although the detailed structure of the diiron core of **X** remains unknown, EXAFS and ^{17}O, ^1H, and ^2H ENDOR data are most consistent with a diiron unit with a short (2.5-Å) Fe−Fe distance, at least one bridging O^{2-}, two other single-atom bridges (O atoms from oxo, hydroxyo, or carboxylate), and an O_2-derived terminal hydroxo or water ligand to the Fe(III) site.[32,50−52]

That **X** is kinetically competent to be the Y122-oxidizing intermediate when the reaction is carried out with excess Fe(II) (to provide a source of the extra electron) was shown by a combination of stopped-flow absorption measurements, which gave accurate kinetics of formation of the Y122 radical (Y122•); RFQ Mössbauer experiments, which allowed the kinetics of formation and decay of **X** to be defined; and RFQ EPR experiments, which allowed both formation of Y122• and formation and decay of **X** to be monitored.[44] Kinetic data from the three methods were found to agree remarkably well, establishing the utility of RFQ Mössbauer spectroscopy for enzyme kinetics. In this case, the subspectra of the three principal iron species present in the RFQ samples [the Fe(II) reactant, the Fe(III)/Fe(IV) cluster **X**, and the (μ-oxo)-diiron(III) product] were sufficiently well-resolved that quantitation of each was relatively straightforward. That **X** is the Y122 oxidant was further supported by the finding that the lifetime of the intermediate is greater (5−10-fold) in the Y122F variant of R2.[43,53]

RFQ Mössbauer spectroscopy played an equally important role in characterization of the reductant-sensitive, 560-nm-absorbing intermediate.[54] Initially, the species was assigned as a μ-peroxodiiron(III) intermediate,[43] but RFQ Mössbauer experiments failed to reveal spectral features that correlate kinetically with the optical absorption, suggesting that it does not arise from an iron complex.[45] The subsequent proposal that the absorbing species is a cation radical derived from one-electron oxidation of the near-surface tryptophan 48 (W48) side chain during formation of **X** was demonstrated through a combination of sequential-mixing RFQ EPR experiments, careful analysis of field-dependent Mössbauer spectra,[54] and site-directed mutagenesis.[55] The RFQ EPR experiments showed that the $g = 2$ EPR intensity is lost upon reduction of the absorbing species with excess Fe(II). Accompanying this loss of intensity, the $g = 2$ region of the spectrum narrows, with features in the "wings" being lost, and the sharp singlet characteristic of **X** appears. This experiment showed that the absorbing species contributes to the total $g = 2$ intensity, consistent with its assignment as a radical. The association of the radical with unusually broad features suggested that it might be experiencing coupling with an additional paramagnetic species, possibly cluster **X**. Indeed, broadening is typical of weakly (dipolar) coupled spins, and the distance of W48 from the diiron cluster (10 Å) is in accordance with the observed dipolar coupling strength. Mössbauer spectroscopy was used to demonstrate that the dipolar interaction of the radical is indeed with **X**. The spectrum of **X** in the presence of the absorbing species exhibits interesting behavior: the fraction of "normal" (i.e., magnetically split) cluster **X** reflected in the Mössbauer spectrum depends on the magnitude of the external magnetic field (Figure 3B). Under the assumption of dipolar coupling between the well-separated ground state of **X** ($S = {}^1/_2$) and $W48^{+\bullet}$ ($S = {}^1/_2$), this behavior was explained. Dipolar coupling leads to four states, of which the energies and spin expectation values as functions of the magnetic field are shown in Figure 3C and D. Because the coupling is weak, all four substates are essentially equally populated at 4.2 K in a weak magnetic field. Two of these states have spin expectation values near zero and give rise to quadrupole doublets, whereas the other two states exhibit their full spin expectation values and give rise to the normal magnetically split subspectra of **X**. However, upon the application of a strong magnetic field (e.g., 8 T), the ground state, which exhibits its full spin expectation value, is almost exclusively populated at 4.2 K (Figure 3D). As a consequence, nearly all of the absorption associated with **X** is

(49) Sturgeon, B. E.; Burdi, D.; Chen, S.; Huynh, B. H.; Edmondson, D. E.; Stubbe, J.; Hoffman, B. M. *J. Am. Chem. Soc.* **1996**, *118*, 7551−7557.
(50) Burdi, D.; Sturgeon, B. E.; Tong, W. H.; Stubbe, J.; Hoffman, B. M. *J. Am. Chem. Soc.* **1996**, *118*, 281−282.
(51) Willems, J.-P.; Lee, H.-I.; Burdi, D.; Doan, P. E.; Stubbe, J.; Hoffman, B. M. *J. Am. Chem. Soc.* **1997**, *119*, 9816−9824.
(52) Burdi, D.; Willems, J.-P.; Riggs-Gelasco, P. J.; Antholine, W. E.; Stubbe, J.; Hoffman, B. M. *J. Am. Chem. Soc.* **1998**, *120*, 12910−12919.
(53) Tong, W. H.; Burdi, D.; Riggs-Gelasco, P. J.; Chen, S.; Edmondson, D. E.; Huynh, B. H.; Stubbe, J.; Han, S.; Arvai, A.; Tainer, J. *Biochemistry* **1998**, *37*, 5840−5848.
(54) Baldwin, J.; Krebs, C.; Ley, B. A.; Edmondson, D. E.; Huynh, B. H.; Bollinger, J. M., Jr. *J. Am. Chem. Soc.* **2000**, *122*, 12195−12206.
(55) Krebs, C.; Chen, S.; Baldwin, J.; Ley, B. A.; Patel, U.; Edmondson, D. E.; Huynh, B. H.; Bollinger, J. M., Jr. *J. Am. Chem. Soc.* **2000**, *122*, 12207−12219.

contributed by the normal paramagnetic features. The demonstration of this unusual field dependence is the most direct evidence that **X** is weakly (dipolar) coupled to a nearby paramagnetic center (for a more detailed discussion, see ref 55). Together with the stopped-flow and EPR results and the observation that the 560-nm-absorbing species does not form in the W48F variant of R2, the Mössbauer data corroborate the proposal that $W48^{+\bullet}$ forms concomitantly with **X**. Similar analysis of a distinct "diradical" species that forms in the W48F variant of R2 led to even more detailed insight.[55]

After the initial work on cofactor assembly in R2, two different groups, one led by Lippard and the other by Lipscomb, used RFQ Mössbauer spectroscopy to investigate the mechanism of O_2 activation by soluble methane monooxygenase (sMMO).[40,56] The active site of sMMO is a carboxylate-bridged diiron cluster that is remarkably similar to that in R2 and is contained in the enzyme's hydroxylase component (sMMOH) within a four-helix bundle that also closely resembles the cluster-binding region of R2.[57] Activation of O_2 by the diiron(II) cluster leads to hydroxylation of methane[58] and concomitant oxidation of the cluster to the diiron(III) state (Scheme 1).[59,60] A reductase component (sMMOR) reduces the cluster back to diiron(II) using electrons from NADH. A coupling protein (sMMOB) serves to coordinate the oxidative and reductive half-reactions and must bind to reduced [diiron(II)] sMMOH for the latter to exhibit full reactivity toward O_2. Upon mixing of reduced sMMOH with O_2 (in the presence of sMMOB), two intermediates, designated **P** or $\mathbf{H}_{peroxo}$ (hereafter, **P**, for its greater simplicity) and **Q**, were detected.[40,56] The kinetics of formation and decay of the intermediates indicate that **P** forms first and decays to **Q**.[41] The acceleration of the decay of **Q** upon its mixing with methane and a large deuterium kinetic isotope effect (KIE) on this decay suggest that **Q** is the species that hydroxylates methane (or initiates hydroxylation by C−H bond cleavage).[61,62] **P** exhibits a broad absorption feature centered near 700 nm and a sharp Mössbauer quadrupole doublet with unusual isomer shift, $\delta = 0.66$ mm/s. High-field Mössbauer data established that the complex has a diamagnetic ($S = 0$) ground state, and **P** was proposed to be a peroxodiiron(III) species.[40] Further spectroscopic characterization has not been forthcoming, but absorption and resonance Raman data on a complex with similar optical and Mössbauer signatures in the W48F/D84E variant of R2[63] and DFT calculations on this system are most consistent with the μ-1,2-peroxodiiron(III) formulation (vide infra),[64] as has also been proposed for **P**.[65] **Q** exhibits absorption features in the 330−430 nm range[66] and a broad Mössbauer quadrupole doublet with unusual parameters. The features of **Q** in *Methylosinus trichosporium* OB3b sMMOH were fitted to one quadrupole doublet, $\delta = 0.17$ mm/s and $\Delta E_Q = 0.53$ mm/s,[56] and those of **Q** in *Methylococcus capsulatus* (Bath) sMMOH to two quadrupole doublets with slightly different parameters ($\delta = 0.14$ mm/s, $\Delta E_Q = 0.55$ mm/s; $\delta = 0.21$ mm/s, $\Delta E_Q = 0.68$ mm/s).[40] The average of these parameters compares well with those found for **Q** in *M. trichosporium* sMMOH. As with **P**, the spectrum of **Q** in a strong applied field revealed it to be diamagnetic.[41,56] The low isomer shift values indicate that the Fe sites of **Q** are formally in the 4+ oxidation state. This assignment was corroborated by the observation that cryoreduction of **Q** leads to a species, termed $\mathbf{Q}_X$, with Mössbauer parameters similar to those observed for cluster **X** in R2 (Table 1).[67] EXAFS experiments revealed that the Fe−Fe separation is a remarkably short 2.46 Å. In addition, one short Fe−O_{oxo} bond distance of 1.77 Å per iron was found, which led to the suggestion that **Q** has an asymmetric bis-(μ-oxo)diiron(IV) core structure.[31]

RFQ Mössbauer spectroscopy was used by Huynh and coworkers to study the ferritin ferroxidase reaction (Scheme 1).[68] Each of the 24 subunits of ferritin, the iron-storage protein,[69,70] contains a site, the so-called ferroxidase site, at which Fe(II) is oxidized to Fe(III) for subsequent translocation to the mineral core at the inside of ferritin. The ferroxidase active site is a carboxylate-rich, dinuclear site similar to those in other diiron enzymes.[71,72] In the reaction of H-ferritin with Fe(II) and O_2, the formation of distinct oxo/hydroxyo-bridged Fe(III) multimers was observed in the early phase of the reaction by RFQ Mössbauer spectroscopy. These were identified as three dimers (based on their diamagnetic ground states) and one trimer (identified by the magnetic field dependence of the individual Fe sites).[73] More insight into the mechanism of the ferroxidase reaction was obtained with frog M-ferritin. A reaction intermediate was detected initially by stopped-flow absorption spectroscopy

(56) Lee, S. K.; Fox, B. G.; Froland, W. A.; Lipscomb, J. D.; Münck, E. *J. Am. Chem. Soc.* **1993**, *115*, 6450−6451.
(57) Rosenzweig, A. C.; Frederick, C. A.; Lippard, S. J.; Nordlund, P. *Nature* **1993**, *366*, 537−543.
(58) Dalton, H. *Adv. Appl. Microbiol.* **1980**, *26*, 71−87.
(59) Wallar, B. J.; Lipscomb, J. D. *Chem. Rev.* **1996**, *96*, 2625−2657.
(60) Merkx, M.; Kopp, D. A.; Sazinsky, M. H.; Blazyk, J. L.; Müller, J.; Lippard, S. J. *Angew. Chem., Int. Ed.* **2001**, *40*, 2782−2807.
(61) Nesheim, J. C.; Lipscomb, J. D. *Biochemistry* **1996**, *35*, 10240−10247.
(62) Valentine, A. M.; Stahl, S. S.; Lippard, S. J. *J. Am. Chem. Soc.* **1999**, *121*, 3876−3887.
(63) Solomon, E. I.; Brunold, T. C.; Davis, M. I.; Kemsley, J. N.; Lee, S. K.; Lehnert, N.; Neese, F.; Skulan, A. J.; Yang, Y.-S.; Zhou, J. *Chem. Rev.* **2000**, *100*, 235−349.
(64) Skulan, A. J.; Brunold, T. C.; Baldwin, J.; Saleh, L.; Bollinger, J. M., Jr.; Solomon, E. I. *J. Am. Chem. Soc.* **2004**, *126*, 8842−8855.
(65) Dunietz, B. D.; Beachy, M. D.; Cao, Y.; Whittington, D. A.; Lippard, S. J.; Friesner, R. A. *J. Am. Chem. Soc.* **2000**, *122*, 2828−2839.
(66) Lee, S. K.; Nesheim, J. C.; Lipscomb, J. D. *J. Biol. Chem.* **1993**, *268*, 21569−21577.
(67) Valentine, A. M.; Tavares, P.; Pereira, A. S.; Davydov, R.; Krebs, C.; Hoffman, B. M.; Edmondson, D. E.; Huynh, B. H.; Lippard, S. J. *J. Am. Chem. Soc.* **1998**, *120*, 2190−2191.
(68) Krebs, C.; Edmondson, D. E.; Huynh, B. H. *Methods Enzymol.* **2002**, *354*, 436−454.
(69) Waldo, G. S.; Theil, E. C. In *Comprehensive Supramolecular Chemistry*; Suslick, K. S., Ed.; Elsevier: Oxford, U.K., 1996; Vol. 5, pp 65−89.
(70) Harrison, P. M.; Arosio, P. *Biochim. Biophys. Acta* **1996**, *1275*, 161−203.
(71) Ha, Y.; Shi, D.; Small, G. W.; Theil, E. C.; Allewell, N. M. *J. Biol. Inorg. Chem.* **1999**, *4*, 243−256.
(72) Lawson, D. M.; Artymiuk, P. J.; Yewdall, S. J.; Smith, J. M. A.; Livingstone, J. C.; Treffry, A.; Luzzago, A.; Levi, S.; Arosio, P.; Cesareni, G.; Thomas, C. D.; Shaw, W. V.; Harrison, P. M. *Nature* **1991**, *349*, 541−544.
(73) Pereira, A. S.; Tavares, P.; Lloyd, S. G.; Danger, D.; Edmondson, D. E.; Theil, E. C.; Huynh, B. H. *Biochemistry* **1997**, *36*, 7917−7927.

(λ_{max} = 650 nm)[74] and subsequently by RFQ Mössbauer spectroscopy.[75] On the basis of the Mössbauer parameters (δ = 0.62 mm/s, ΔE_Q = 1.08 mm/s) and the fact that it has a diamagnetic ground state, this species was proposed to be a peroxodiiron(III) species, termed $\mathbf{F}_{peroxo}$. Moreover, variable-temperature, variable-field Mössbauer spectroscopy was used to determine the exchange coupling constant, $J = (+75 \pm 10)$ cm^{-1} (as defined in eq 8).[76] Further insight into the geometric structure of $\mathbf{F}_{peroxo}$ was obtained from RFQ resonance Raman[36] and RFQ X-ray absorption studies.[34] The detection of O-isotope sensitive bands assigned to ν(Fe−O) and ν(O−O) is consistent with a μ-1,2-bridging mode of the peroxide ligand. The Fe−Fe distance of 2.53 Å, detected by RFQ EXAFS spectroscopy, is significantly shorter than those of μ-1,2-peroxodiiron(III) enzyme reaction intermediates[35] and model complexes.[77−80] The unusual core structure was proposed to result in a stronger O−O bond, which could favor release of hydrogen peroxide, as opposed to the O−O bond cleavage observed for other diiron proteins that form high-valent Fe species (R2 and sMMOH).[34] Formation of H_2O_2 as a product of the ferroxidase reaction was demonstrated.[81,82] In a more recent study, the amount of H_2O_2 generated during the ferroxidase reaction, determined spectrophotometrically, was correlated quantitatively to the amount of $\mathbf{F}_{peroxo}$, determined by RFQ Mössbauer spectroscopy.[83] Furthermore, it was shown that decay of $\mathbf{F}_{peroxo}$ parallels the formation of multiple (at least three) distinct oxo/hydroxo-bridged diiron(III) species, which are subsequently translocated to the mineral core.[75,83]

A peroxodiiron(III) complex was also detected in the plant enzyme stearoyl acyl carrier protein Δ^9 desaturase (Δ^9-D),[84,85] which activates O_2 at a carboxylate-bridged diiron(II) cluster almost identical to those in R2 and sMMOH to introduce a cis double bond between carbons 9 and 10 of stearic acid bound as thioester to acyl carrier protein (Scheme 1).[86] The intermediate accumulates in the reaction of O_2 only with chemically (artificially) reduced enzyme, not with the enzymatically (naturally) reduced protein. Its decay is not associated with substrate desaturation and is too slow ($t_{1/2}$ = 30 min at 20 °C) to be on the productive pathway. In fact, no chemically and kinetically competent oxidized iron intermediate has yet been detected in this fascinating reaction. Success in this endeavor would be of tremendous value to our understanding of protein tuning of the diiron carboxylate unit for diverse oxidation reactivities.

More recent work on the R2 reaction has focused on the use of amino acid substitutions to define the most important structural determinants of its one-electron-oxidation outcome, Y122$^\bullet$ production (as opposed to the two-electron oxidations mediated by sMMO and Δ^9-D). Whereas a comprehensive account of these studies is beyond the scope of this article, a brief summary reveals the central role played by RFQ Mössbauer spectroscopy. The fundamental question has been whether R2 and the other O_2-activating diiron carboxylate proteins, despite mediating different reaction outcomes, follow a common initial pathway through one or more common intermediate or, to the contrary (as suggested by the ferritin work[34] and even earlier by Fox, Loehr, and coworkers[87]), promote formation of O_2 adducts with distinct structures and reactivities as a means of dictating different outcomes. For the R2 reaction, the question is whether the precursors to cluster **X** are similar or identical to the peroxodiiron(III) complex **P**, the diiron(IV) complex **Q**, both, or neither. Diiron intermediates of this overall oxidation state (more oxidized than **X** by one electron) might or might not accumulate in the R2 reaction. An early study presented some evidence for accumulation of a **P**-like complex very early in the reaction of diiron(II) R2 with O_2.[88] Long-wavelength absorption and a feature at approximately +1.4 mm/s, which is at the position of the high-energy line of **P**, were detected. A later study failed to detect these features (or found them to be much less intense), and presented kinetic data suggesting that the precursor to the **X**-W48$^{+\bullet}$ diradical state should not accumulate to greater than ~0.1 equiv.[54] The apparently conservative substitution of Fe1 ligand D84 with E, which amounts to addition of a single methylene unit to the linker between the protein backbone and the carboxylate ligand and which renders the amino acid iron ligands of R2 identical with those in sMMOH, allows nearly 1 equiv of a peroxodiiron(III) complex to accumulate.[89] The complex has the characteristic high isomer shift (δ = 0.63 mm/s) and long-wavelength absorption (λ_{max} = 700 nm, $\epsilon_{700} \approx 1800$ M^{-1}cm^{-1}). Decay of the complex was found to lead to production of 1 equiv of Y122$^\bullet$ in R2-D84E. However, when the additional substitution of W48 with F was introduced to block transfer of the extra electron, decay of the intermediate was found to result primarily in hydroxylation of the ϵ carbon of the nearby F208 by an O-atom-insertion (i.e., monooxygenase-like) mechanism.[90] In the R2-W48F/D84E double variant, the lifetime of the peroxodiiron(III) complex was sufficient to permit its cryosolventless trapping and resonance

(74) Fetter, J.; Cohen, J.; Danger, D.; Sanders-Loehr, J.; Theil, E. C. *J. Biol. Inorg. Chem.* **1997**, *2*, 652−661.
(75) Pereira, A. S.; Small, G. W.; Krebs, C.; Tavares, P.; Edmondson, D. E.; Theil, E. C.; Huynh, B. H. *Biochemistry* **1998**, *37*, 9871−9876.
(76) Krebs, C.; Bollinger, J. M., Jr.; Theil, E. C.; Huynh, B. H. *J. Biol. Inorg. Chem.* **2002**, *7*, 863−869.
(77) Kim, K.; Lippard, S. J. *J. Am. Chem. Soc.* **1996**, *118*, 4914−4915.
(78) Dong, Y.; Yan, S.; Young, V. G., Jr.; Que, L., Jr. *Angew. Chem., Int. Ed. Engl.* **1996**, *35*, 618−620.
(79) Ookubo, T.; Sugimoto, H.; Nagayama, T.; Masuda, H.; Sato, T.; Tanaka, K.; Maeda, Y.; Okawa, H.; Hayashi, Y.; Uehara, A.; Suzuki, M. *J. Am. Chem. Soc.* **1996**, *118*, 701−702.
(80) Dong, Y.; Zang, Y.; Kauffmann, K. E.; Shu, L.; Wilkinson, E. C.; Münck, E.; Que, L., Jr. *J. Am. Chem. Soc.* **1997**, *119*, 12683−12684.
(81) Xu, B.; Chasteen, N. D. *J. Biol. Chem.* **1991**, *266*, 19965−19970.
(82) Waldo, G. S.; Theil, E. C. *Biochemistry* **1993**, *32*, 13262−13269.
(83) Jameson, G. N. L.; Jin, W.; Krebs, C.; Pereira, A. S.; Tavares, P.; Liu, X.; Theil, E. C.; Huynh, B. H. *Biochemistry* **2002**, *41*, 13435−13443.
(84) Broadwater, J. A.; Ai, J.; Loehr, T. M.; Sanders-Loehr, J.; Fox, B. G. *Biochemistry* **1998**, *37*, 14664−14671.
(85) Broadwater, J. A.; Achim, C.; Münck, E.; Fox, B. G. *Biochemistry* **1999**, *38*, 12197−12204.
(86) Fox, B. G.; Lyle, K. S.; Rogge, C. E. *Acc. Chem. Res.* **2004**, *37*, 421−429.
(87) Fox, B. G.; Shanklin, J.; Ai, J.; Loehr, T. M.; Sanders-Loehr, J. *Biochemistry* **1994**, *33*, 12776−12786.
(88) Tong, W. H.; Chen, S.; Lloyd, S. G.; Edmondson, D. E.; Huynh, B. H.; Stubbe, J. *J. Am. Chem. Soc.* **1996**, *118*, 2107−2108.
(89) Bollinger, J. M., Jr.; Krebs, C.; Vicol, A.; Chen, S.; Ley, B. A.; Edmondson, D. E.; Huynh, B. H. *J. Am. Chem. Soc.* **1998**, *120*, 1094−1095.

Raman characterization.[91] Vibrational frequencies, their shifts with ^{17}O- and ^{18}O-isotopic substitution, and especially the resonant enhancement profiles of the two observed vibrational modes are most consistent with a μ-1,2-peroxodiiron(III) structure,[63] as originally proposed for **P**. The accumulation of a **P**-like complex in an R2 variant and demonstration that it can mediate either the normal R2 outcome or a more sMMO-like outcome seem to favor the notion of a common initial pathway for the two enzymes. However, because formation of **X** from the **P**-like complex in the R2-D84E reaction was never demonstrated, the possibility remained that the D84E ligand substitution, rather than merely stabilizing the same intermediate that forms with the wild-type ligand set, actually *causes* the peroxodiiron(III) complex to form in preference to a different species that forms with the wild-type ligand set. Therefore, the reactions of R2 variants with electron transfer to the cluster disabled but the wild-type ligand set retained were examined by RFQ Mössbauer spectroscopy. Initially, the double variant having electron transfer from both outside and inside the protein disabled (by the W48F and Y122F substitutions, respectively) was interrogated. Mössbauer spectra of RFQ samples clearly showed features not attributable to reactants or products, but they appeared also to reflect heterogeneity, even at early reaction times. As a tool to resolve the features of the complex(es) specifically capable of converting to **X**, the strategy of triggering electron transfer with a small molecule was explored. Experiments with R2-W48A, in which replacement of the 3-indolylmethyl side chain by methyl was intended to create a cavity into which indole compounds could bind, demonstrated the efficacy of the method.[92] A more extensive series of stopped-flow and RFQ experiments with R2-W48A/Y122F showed that an intermediate state forms rapidly upon mixing the diiron(II) complex with O_2, decays slowly in the absence of a mediator of electron transfer, and is triggered to convert to **X** upon its mixing with mediator (3-methylindole).[93] The Mössbauer features lost in the triggering to **X** (Figure 3E) and those developing in the initial mix with O_2 are essentially indistinguishable. Analysis of the features suggested the presence of at least two diiron species (Figure 3E, spectrum c). The outer features were analyzed as one quadrupole doublet ($\delta = 0.45$ mm/s, $\Delta E_Q = 1.53$ mm/s), and the inner features as either one broad quadrupole doublet ($\delta = 0.52$ mm/s, $\Delta E_Q = 0.55$ mm/s) or two quadrupole doublets ($\delta = 0.60$ mm/s, $\Delta E_Q = 0.53$ mm/s; $\delta = 0.43$ mm/s, $\Delta E_Q = 0.55$ mm/s), with one (the first) having the same intensity as the outer doublet. The fact that the state behaves as a single kinetic entity (all features developing and decaying together in constant proportion) suggests that the two or more constituent complexes are in rapid (with respect to formation and decay) equilibrium. Regardless of which analysis is correct, the Mössbauer parameters and lack of magnetic hyperfine interactions for each species are indicative of antiferromagnetically coupled diiron(III) clusters. The fact that both complexes convert to **X** upon triggering with 3-methylindole indicates that they are more oxidized than **X** by one electron, suggesting the presence of a peroxide ligand. More detailed structural insight awaits characterization by other methods, but the Mössbauer and absorption spectra of the state show that neither constituent is similar to the known μ-1,2-peroxodiiron(III) complexes such as that formed in R2-D84E nor to the diiron(IV) complex **Q**. Although partially successful in its aim of characterizing the precursor to cluster **X**, this study also shows two important limitations of Mössbauer spectroscopy in the study of iron enzyme mechanisms. In this case, the rather low resolution precluded unambiguous deduction of subspectra of component species. More importantly, even if these had been definitively assigned, they would not, in the absence of additional spectroscopic or computational studies, have provided structural insight at the level of detail necessary to understand precisely how the intermediate state in question differs from previously studied diiron$-O_2$ intermediates.

Oxygen Activation by an Fe(II)- and α-Ketoglutarate-Dependent Dioxygenase, TauD. The α-ketoglutarate (αKG)-dependent dioxygenases are a large and functionally diverse family of enzymes that catalyze important reactions in the biosynthesis of antibiotics and collagen, the degradation of xenobiotics, and the biosynthesis of antioxidants.[94,95] Recently, two important reactions relevant to human biochemistry were found to be catalyzed by αKG-dependent dioxygenases: repair of methylated DNA in bacteria and humans[96] and cellular sensing of oxygen and initiation of response to hypoxia.[97−100] Members of the Fe(II):αKG enzyme family couple the reductive activation of dioxygen to the hydroxylation of their substrates and the decarboxylation of the cosubstrate, αKG. In each case, the reaction is carried out at a mononuclear non-heme Fe center, which is facially coordinated by a conserved $(His)_2(Asp/Glu)$ motif from the protein.[101] The mechanism of this reaction is thought to be conserved for all αKG-dependent dioxygenases,[63,95] and a consensus mechanism (Scheme 2), involving intermediates **I**−**IV**, has repeatedly been proposed for many years.[102,103]

(90) Baldwin, J.; Voegtli, W. C.; Khidekel, N.; Moënne-Loccoz, P.; Krebs, C.; Pereira, A. S.; Ley, B. A.; Huynh, B. H.; Loehr, T. M.; Riggs-Gelasco, P. J.; Rosenzweig, A. C.; Bollinger, J. M., Jr. *J. Am. Chem. Soc.* **2001**, *123*, 7017−7030.
(91) Moënne-Loccoz, P.; Baldwin, J.; Ley, B. A.; Loehr, T. M.; Bollinger, J. M., Jr. *Biochemistry* **1998**, *37*, 14659−14663.
(92) Saleh, L.; Kelch, B. A.; Pathickal, B. A.; Baldwin, J.; Ley, B. A.; Bollinger, J. M., Jr. *Biochemistry* **2004**, *43*, 5943−5952.
(93) Saleh, L.; Krebs, C.; Ley, B. A.; Naik, S.; Huynh, B. H.; Bollinger, J. M., Jr. *Biochemistry* **2004**, *43*, 5953−5964.
(94) Hausinger, R. P. *Crit. Rev. Biochem. Mol. Biol.* **2004**, *39*, 21−68.
(95) Costas, M.; Mehn, M. P.; Jensen, M. P.; Que, L., Jr. *Chem. Rev.* **2004**, *104*, 939−986.
(96) Trewick, S. C.; Henshaw, T. F.; Hausinger, R. P.; Lindahl, T.; Sedgwick, B. *Nature* **2002**, *419*, 174−178.
(97) Ivan, M.; Kondo, K.; Yang, H.; Kim, W.; Valiando, J.; Ohh, M.; Salic, A.; Asara, J. M.; Lane, W. S.; Kaelin, W. G., Jr. *Science* **2001**, *292*, 464−468.
(98) Jaakkola, P.; Mole, D. R.; Tian, Y.-M.; Wilson, M. I.; Gielbert, J.; Gaskell, S. J.; von Kriegsheim, A.; Hebestreit, H. F.; Mukherji, M.; Schofield, C. J.; Maxwell, P. H.; Pugh, C. W.; Ratcliffe, P. J. *Science* **2001**, *292*, 468−472.
(99) Epstein, A. C. R.; Gleadle, J. M.; McNeill, L. A.; Hewitson, K. S.; O'Rourke, J.; Mole, D. R.; Mukherji, M.; Metzen, E.; Wilson, M. I.; Dhanda, A.; Tian, Y.-M.; Masson, N.; Hamilton, D. L.; Jaakkola, P.; Barstead, R.; Hodgkin, J.; Maxwell, P. H.; Pugh, C. W.; Schofield, C. J.; Ratcliffe, P. J. *Cell* **2001**, *107*, 43−54.
(100) Bruick, R. K.; McKnight, S. L. *Science* **2001**, *294*, 1337−1340.
(101) Que, L., Jr. *Nat. Struct. Biol.* **2000**, *7*, 182−184.

Scheme 2. Proposed Reaction Mechanism of the Fe(II) and α-Ketoglutarate-Dependent Dioxygenases, Adapted for the Specific Case of the Enzyme Taurine:α-Ketoglutarate Dioxygenase (TauD)

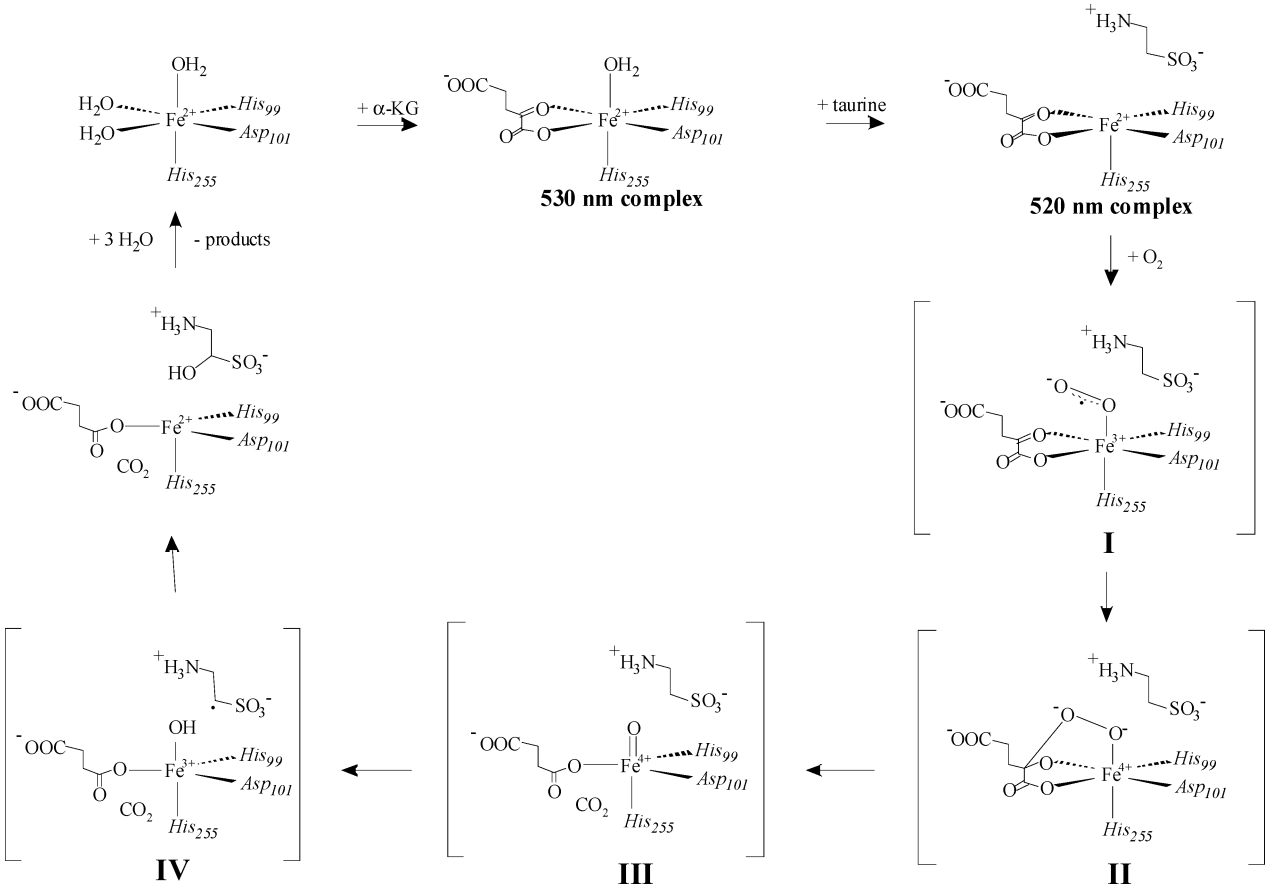

Whereas many studies on a number of different enzymes[104−107] and model systems[107,108] provided evidence for this mechanism, none of the intermediates **I**−**IV** had been directly detected until recently.

Taurine:α-ketoglutarate dioxygenase (TauD) from *Escherichia coli* is a member of this large enzyme family. It catalyzes hydroxylation of C1 of taurine (2-aminoethane-1-sulfonic acid) and other organosulfonates to initiate elimination of sulfite.[109] Ground-breaking work by the Hausinger group revealed TauD to be among the best candidates in this family for mechanistic dissection by RFQ Mössbauer spectroscopy and related methods.[110] Stopped-flow absorption and RFQ Mössbauer experiments provided evidence for the accumulation of two intermediate states upon reaction of the TauD:Fe(II):αKG:taurine quaternary complex with O_2 (Scheme 2).[111] The first state is associated with absorption in the UV regime ($\lambda_{max} \approx 320$ nm) and a Mössbauer quadrupole doublet (Figure 4A) with $\delta = 0.31$ mm/s and $\Delta E_Q = 0.88$ mm/s (theoretical simulation is shown in red). This intermediate is termed **J**. The second state is characterized by a Mössbauer quadrupole doublet characteristic of high-spin Fe(II) and an absence of UV/visible absorption, suggesting that it is most likely a TauD:Fe(II):product(s) complex.[112] The rate-limiting step under the conditions examined (5 °C, $[O_2] > 200$ μM) is regeneration of the quaternary complex from this second intermediate. The low isomer shift of **J** suggested that it has an oxidation state greater than 3+, but the value seemed too high for 4+. Exposure of samples containing high levels of **J** to γ-irradiation at 77 K (cryoreduction) monitored by EPR and Mössbauer spectroscopies was shown to convert it to one (or more) high-spin Fe(III) complex(es), establishing the formal oxidation state of **J** as 4+.[111]

The assignment of **J** as formally Fe(IV) still left several possibilities for its position within the consensus mechanism for the Fe(II):αKG family. To narrow the possibilities, 1,1-

(102) Hobza, P.; Hurych, J.; Zahradnik, R. *Biochim. Biophys. Acta* **1973**, *304*, 466−472.
(103) Hanauske-Abel, H. M.; Günzler, V. *J. Theor. Biol.* **1982**, *94*, 421−455.
(104) Valegard, K.; Terwisscha van Scheltinga, A. C.; Lloyd, M. D.; Hara, T.; Ramaswamy, S.; Perrakis, A.; Thompson, A.; Lee, H.-J.; Baldwin, J. E.; Schofield, C. J.; Hajdu, J.; Andersson, I. *Nature* **1998**, *394*, 805−809.
(105) Wu, M.; Moon, H.-S.; Begley, T. P.; Myllyharju, J.; Kivirikko, K. I. *J. Am. Chem. Soc.* **1999**, *121*, 587−588.
(106) Zhou, J.; Kelly, W. L.; Bachmann, B. O.; Gunsior, M.; Townsend, C. A.; Solomon, E. I. *J. Am. Chem. Soc.* **2001**, *123*, 7388−7398.
(107) Ho, R. Y. N.; Mehn, M. P.; Hegg, E. L.; Liu, A.; Ryle, M. J.; Hausinger, R. P.; Que, L., Jr. *J. Am. Chem. Soc.* **2001**, *123*, 5022−5029.
(108) Chiou, Y.-M.; Que, L., Jr. *J. Am. Chem. Soc.* **1995**, *117*, 3999−4013.
(109) Eichhorn, E.; van der Ploeg, J. R.; Kertesz, M. A.; Leisinger, T. *J. Biol. Chem.* **1997**, *272*, 23031−23036.
(110) Ryle, M. J.; Padmakumar, R.; Hausinger, R. P. *Biochemistry* **1999**, *38*, 15278−15286.
(111) Price, J. C.; Barr, E. W.; Tirupati, B.; Bollinger, J. M., Jr.; Krebs, C. *Biochemistry* **2003**, *42*, 7497−7508.
(112) Price, J. C.; Barr, E. W.; Hoffart, L. M.; Krebs, C.; Bollinger, J. M., Jr., manuscript in preparation.

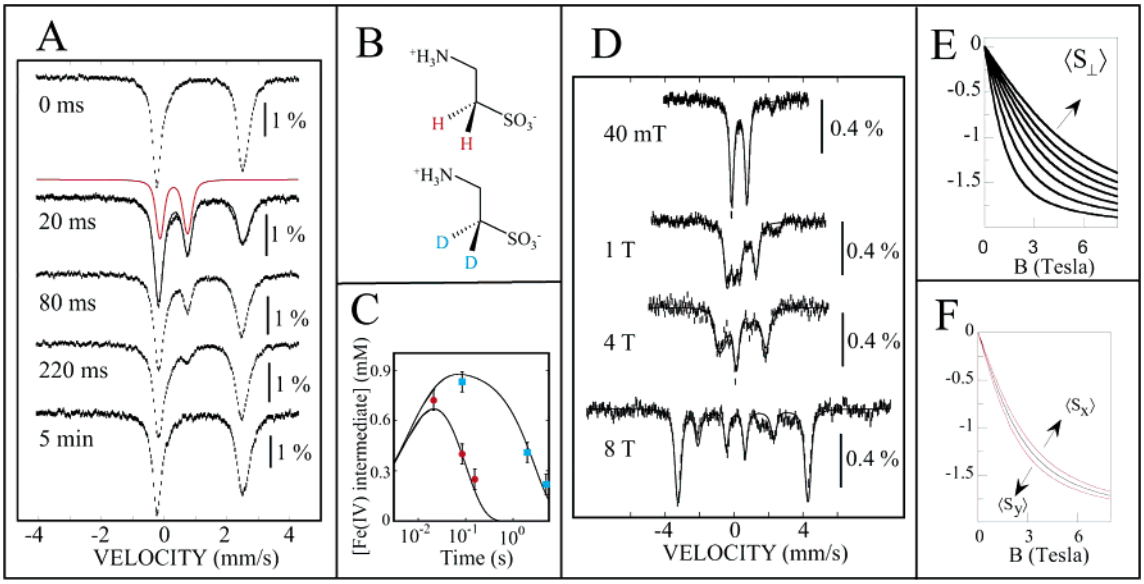

Figure 4. (A) 4.2 K/40-mT Mössbauer spectra of RFQ samples from the reaction of the TauD:Fe(II):αKG:taurine complex with O_2. The reaction times are shown. The spectra are adapted from Price et al.[111] A simulation of the spectrum of **J** according to parameters in the text is shown in red. (B) Structures of 1,1-[^{1}H]$_2$-taurine and 1,1-[^{2}H]$_2$-taurine. (C) Concentration of **J**, determined from 4.2 K/40-mT Mössbauer spectra (red, 1,1-[^{1}H]$_2$-taurine; blue, 1,1-[^{2}H]$_2$-taurine) and theoretical concentrations of **J** obtained by kinetic simulation. The figure is adapted from Price et al.[113] (D) Field-dependent Mössbauer reference spectra of **J** recorded at 4.2 K in magnetic fields of (a) 40 mT, (b) 0.5 T, (c) 1 T, and (d) 8 T. Simulations were carried out using the parameters given in Table 2. (E) Spin expectation values of an $S = 2$ system with $E/D = 0$, calculated for different D values (from 5.0 to 20.0 cm^{-1} in 2.5 cm^{-1} increments). The arrow indicates increasing D. (F) Spin expectation values of an $S = 2$ system with $D = +10.5$ cm^{-1}, calculated for $E/D = 0$ (black) and $E/D = 0.03$ (red).

[^{2}H]$_2$-taurine (Figure 4B) was synthesized and used to test for a deuterium kinetic isotope effect (KIE) on formation or decay of the intermediate (or both).[113] A large normal KIE ($k_H/k_D \approx 35$) on decay of **J**, but no KIE on its formation, was observed. This result was shown both by stopped-flow absorption measurements and, more notably, by RFQ Mössbauer spectroscopy (Figure 4C). To our knowledge, this study represents the first use of Mössbauer spectroscopy for determination of a KIE in an enzyme reaction. The result suggests that **J** is responsible for cleavage of the C1−[^{1,2}H] bond, making the most likely identity of the complex the Fe(IV)═O^{2-} species, **III**, in Scheme 2. This assignment was subsequently validated in technically brilliant, cryogenic, continuous-flow resonance Raman experiments by Proshlyakov et al., who detected a band at 821 cm^{-1} that shifts to 787 cm^{-1} upon formation of the intermediate with $^{18}O_2$ and ascribed this band on the basis of extensive precedent to the Fe−O stretch.[114] Further confirmation was then provided by RFQ EXAFS measurements, in which a ligand scatterer 1.62 Å from the Fe was detected and was assigned to the O of an Fe(IV)═O^{2-} moiety.[33] In the latter study, samples were examined by Mössbauer spectroscopy before and after the X-ray absorption measurements, to determine the amount of **J** present in the sample (an important constraint for analysis of the EXAFS data) and to address the degree of photoreduction during the XAS experiments.

To study the electronic structure of **J** further, Mössbauer spectra were recorded at 4.2 K in varying externally applied magnetic fields. Reference spectra of **J** were obtained by subtracting experimental spectra (recorded under identical conditions) of the TauD:Fe(II):αKG:taurine starting complex from those of a 20-ms freeze-quenched sample; the relative amount of the TauD:Fe(II):αKG:taurine complex is 46%, as determined from the 40-mT spectrum (Figure 4A). The spectra of **J** obtained according to this procedure (Figure 4D) provide detailed insight into the nature of the electronic ground state, as they allow for the determination of the spin state of the Fe center and the ZFS parameters, D and E/D.

The fact that **J** gives rise to a quadrupole doublet in a weak (40-mT) magnetic field but displays increasing magnetic splitting with increasing externally applied magnetic field is typical of a paramagnetic species with (nearly) axial integer-spin electronic ground state and $D > 0$ (Figure 2B). The 8-T spectrum exhibits six sharp lines with peak separations that reflect an effective magnetic field of ∼24 T experienced by the ^{57}Fe nucleus, corresponding to an internal magnetic field of ∼32 T oriented antiparallel to the externally applied 8-T field. The **A** tensor of ^{57}Fe is dominated by the Fermi contact term, which is typically −20 to −22 T, leading to an estimate for $\langle S \rangle$ of 1.5 at 8 T. This spin expectation value requires that **J** have an electronic ground state with $S \geq 2$. Because **J** contains a single Fe center, an $S = 2$ state is most likely and was assumed for the simulations discussed below. An $S = 3$ ground state arising from ferromagnetic coupling between a high-spin Fe(III) site ($S = {}^5/_2$) and a ligand radical ($S = {}^1/_2$) is unlikely, in particular because the isomer shift of **J**, $\delta = 0.31$ mm/s, is smaller than those of high-spin Fe(III) sites in other mononuclear non-heme Fe enzymes, for which isomer shifts in the range $\delta = 0.44-0.56$ mm/s were reported.[115]

(113) Price, J. C.; Barr, E. W.; Glass, T. E.; Krebs, C.; Bollinger, J. M., Jr. *J. Am. Chem. Soc.* **2003**, *125*, 13008−13009.
(114) Proshlyakov, D. A.; Henshaw, T. F.; Monterosso, G. R.; Ryle, M. J.; Hausinger, R. P. *J. Am. Chem. Soc.* **2004**, *126*, 1022−1023.

Table 2. Mössbauer Parameters of **J**, the Fe(IV)═O^{2-} Intermediate of TauD, and Other High-Spin Fe(IV) Complexes

species	δ (mm/s)	ΔE_Q (mm/s)	η	$\mathbf{A}/g_n\beta_n$ (T)[a]	D (cm^{-1})[b]	E/D[b]	ref
J	0.31	−0.88	0	(−18.0, −18.0, −18)[c]	+10.5	0.03	this work
Fe(IV) site of cluster **X**	0.26	−0.6	2.7	(−20, −20, −15)	nd[d]	nd[d]	49
Collins' model compound[e]	-0.04	-0.89	0.15	(−18, −15, −10.8)	−2.6	0.13	117

[a] Given with respect to the spin of the Fe(IV) site, $S = 2$. [b] $S = 2$ was assumed for the simulation. [c] Assumed to be axial. The z component cannot be determined. [d] Not determined because of the $S = {}^1/_2$ ground state of intermediate **X**. [e] [Fe(IV)Cl(η^4-MAC*)]$^-$, with η^4-MAC* = tetra-anion of 1,4,8,11-tetraaza-13,13-diethyl-2,2,5,5,7,7,10,10-octamethyl-3,6,9,12,14-pentaoxocyclotetradecane.

Analysis of the field-dependent spectra of **J** yielded the parameters given in Table 2.[116] The parameters known from the 40-mT spectrum ($\delta = 0.31$ mm/s and $|\Delta E_Q| = 0.88$ mm/s) were fixed. Furthermore, the **A** tensor was assumed to be axial, because of the strong axial oxo ligand.

The dependence of the spin expectation value within the xy plane, $\langle S_\perp \rangle$, of the ground state for an axial ($E/D = 0$) $S = 2$ system with $D > 0$ on the magnetic field correlates strongly with the magnitude of D (Figure 4E). Because the internal magnetic field is proportional to $\langle S \rangle$ (see eq 7), it is possible to determine D accurately from the field dependent spectra. A least-squares fit to the data yields $D = +10.5$ cm^{-1} and $E/D = 0.03$. The spin expectation value is isotropic within the xy plane for $E/D = 0$ (Figure 4F, black line), and becomes slightly anisotropic for increasing E/D (~5% for $E/D = 0.03$; Figure 4F, red lines). Because the simulation is carried out under the assumption of $A_{xx}/g_n\beta_n = A_{yy}/g_n\beta_n$, it follows that the internal magnetic field in the xy plane is nearly isotropic, and as a consequence, the outer lines of the 8-T spectrum are sharp, as is observed experimentally. A least-squares fit in which $A_{xx}/g_n\beta_n$ and $A_{yy}/g_n\beta_n$ are allowed to vary independently does not yield significantly different parameters ($E/D = 0.02$, $A_{xx}/g_n\beta_n = -17.9$ T, and $A_{yy}/g_n\beta_n = -18.1$ T), thus corroborating the assumption that the **A** tensor is essentially axial.

The A values obtained from this analysis ($A_{xx}/g_n\beta_n \approx A_{yy}/g_n\beta_n \approx -18$ T) are close to the Fermi contact term and similar to values observed for heme enzyme Fe(IV)═O^{2-} species[4] and the high-spin Fe(IV) sites in cluster **X** of ribonucleotide reductase and other valence-localized Fe(III)−Fe(IV) species (see Table 1). $A_{zz}/g_n\beta_n$ cannot be determined from the simulations because $\langle S_z \rangle$ is very small, even at 8 T (see Figure 2), and consequently, the simulations are not sensitive to $A_{zz}/g_n\beta_n$.

To gain insight into the electronic and geometric structures of **J**, DFT calculations were performed on a minimal model of the TauD active site (Figure 5) as well as the non-heme

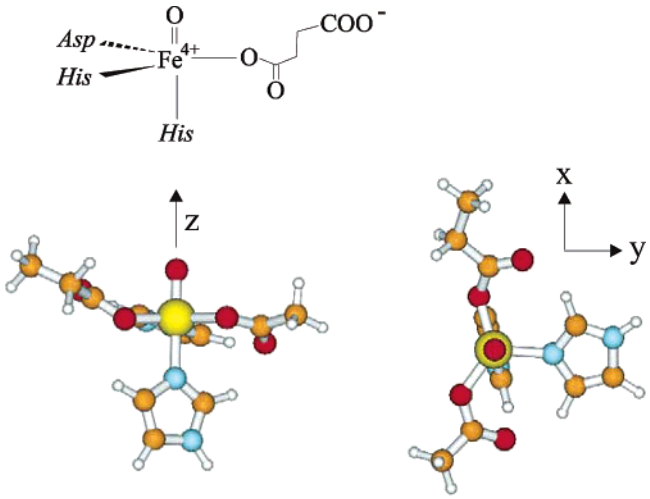

Figure 5. Structural model of intermediate **J** from TauD obtained by DFT calculations.

Fe(IV) complexes of Collins[117] and Que.[118] Because DFT methods can predict Mössbauer parameters with considerable accuracy, the comparison of calculated and experimental values provides a means of validation of structural models for the enzymatic species. In particular, we examined whether a five-coordinate trigonal-bipyramidal structure could explain the $S = 2$ spin state and reproduce the rather unusual Mössbauer parameters observed experimentally.

We judged this trigonal-bipyramidal coordination environment to be a natural starting point for computations, because in this geometry there are two low-lying e sets that can accommodate four unpaired electrons in the observed $S = 2$ configuration. Furthermore, the oxo ligand of **J** indicated by spectroscopic analysis (vide supra) is a good π donor and interactions with this ligand would be expected to push the lower e'' set (xz, yz) up in energy, decreasing the splitting between the e' and e'' levels and further stabilizing the high-spin configuration. This choice of starting configuration does not preclude the examination of a square-pyramidal geometry in which the oxo ligand occupies an equatorial position, as this structure could be obtained during geometry optimizations. However, a square-pyramidal geometry in which the oxo occupies the axial position seems unlikely because of geometric constraints imposed by the His_2−Asp facial triad.

(115) (a) Meyer-Klaucke, W.; Winkler, H.; Schünemann, V.; Trautwein, A. X.; Nolting, H. F.; Haavik, J. *Eur. J. Biochem.* **1996**, *241*, 432−439. (b) Whittaker, J. W.; Lipscomb, J. D.; Kent, T. A.; Münck, E. *J. Biol. Chem.* **1984**, *259*, 4466−4475. (c) Wolfe, M. D.; Altier, D. J.; Stubna, A.; Popescu, C. V.; Münck, E.; Lipscomb, J. D. *Biochemistry* **2002**, *41*, 9611−9626.

(116) A solution of same quality is obtained assuming $S = 1$, yielding parameters almost identical to those in Table 2, except for the following: $D = +6.5$ cm^{-1} and $A_\perp/g_n\beta_n = -33.3$ T. For this simulation, as for the $S = 2$ simulations, D is determined accurately from the field dependence of the internal magnetic field, and $A_\perp/g_n\beta_n$ is determined accurately from the absolute magnitude of the internal magnetic field, knowing the magnitude of $\langle S \rangle$, which, in turn, is determined by D. The larger A value is a consequence of the smaller $\langle S \rangle$, which cannot exceed a value of 1 for an $S = 1$ system. Because the A value is ca. 50% larger than the Fermi contact term and known A values of other Fe(IV) species, we assign $S > 1$ for **J**.

(117) Kostka, K. L.; Fox, B. G.; Hendrich, M. P.; Collins, T. J.; Rickard, C. E. F.; Wright, L. J.; Münck, E. *J. Am. Chem. Soc.* **1993**, *115*, 6746−6757.

(118) Rohde, J.-U.; In, J.-H.; Lim, M. H.; Brennessel, W. W.; Bukowski, M. R.; Stubna, A.; Münck, E.; Nam, W.; Que, L., Jr. *Science* **2003**, *299*, 1037−1039.

(119) Lee, D.; Pierce, B.; Krebs, C.; Hendrich, M. P.; Huynh, B. H.; Lippard, S. J. *J. Am. Chem. Soc.* **2002**, *124*, 3993−4007.

(120) Dong, Y.; Que, L. J.; Kauffmann, K. E.; Münck, E. *J. Am. Chem. Soc.* **1995**, *117*, 11377−11378.

Table 3. Calculated Mössbauer Parameters of **J**, the TauD Fe(IV)═O^{2-} Intermediate, and Other Mononuclear Fe(IV) Complexes

species		δ (mm/s)	ΔE_Q (mm/s)	ref
J	exptl	0.31	−0.88	111
	calcd	0.22	−1.0	this work
Collins' model compound[a]	exptl	−0.04	−0.89	117
	calcd	−0.08	−0.76	this work
Que's model compound[b]	exptl	0.17	1.24	118
	calcd	0.11	1.2	this work

[a] $[(MeCN)Fe(IV)O(Me_4\text{-cyclam})]^{2+}$, with Me_4-cyclam = *N*,*N*′,*N*″,*N*‴-tetramethyl-1,4,8,11-cyclotetraazatetradecane. [b] $[Fe(IV)Cl(\eta^4\text{-MAC*})]^{-}$, with η^4-MAC* = tetra anion of 1,4,8,11-tetraaza-13,13-diethyl-2,2,5,5,7,7,10,10-octamethyl-3,6,9,12,14-pentaoxocyclotetradecane.

Calculations on all systems were performed using the B3LYP hybrid functional. The 6-311G basis set was used for geometry optimizations and EFG determination. Neese's core-properties basis set was used to obtain isomer shifts. The structure of the model of **J** was obtained by an unconstrained geometry optimization. The starting structure for this optimization was a trigonal-bipyramidal geometry, which maintained the classic facial triad exhibited by all members of the αKG-dependent dioxygenase family (Figure 5). Two residues from the facial triad (His/imidazole and Asp/propionate) lie in the equatorial plane. The third (His/imidazole) is in an axial position trans to the Fe(IV)═O^{2-} moiety. The remaining equatorial position is occupied by acetate, which mimics one of the products of the reaction, succinate. This trigonal-bipyramidal geometry was not significantly altered by optimization. Geometries for the synthetic complexes of Collins and Que were taken without modification from the crystal structures.

DFT yields an $S = 2$ ground state for the five-coordinate complex shown in Figure 5. The Fe−O distance of the Fe(IV)═O^{2-} unit is calculated as 1.64 Å. The calculated Mössbauer parameters for the three systems are shown in Table 3. Whereas the magnitude and sign of the quadrupole splitting parameters are well reproduced, the calculated isomer shifts are all lower than the experimental values. The agreement between theory and experiment suggests that **J** might be a trigonal-bipyramidal Fe(IV) species with an axial oxo ligand.

Outlook and Conclusion

The power of Mössbauer spectroscopy as a tool to understand, in particular, the spin coupling of iron ions in polynuclear centers was elegantly demonstrated in the 1970s and 1980s. For these complex clusters, as well as for simpler mononuclear Fe centers, the fundamental parameters (isomer shift and quadrupole splitting) and magnetic-field and temperature dependencies of the Mössbauer spectrum contain important electronic-structural information. Its more recent marriage to the RFQ technique has made Mössbauer spectroscopy a powerful tool for kinetic and mechanistic studies of iron enzymes, in which the value of its capacity for detection and (often) quantification of all iron species in a sample can be invaluable. Clusters with diamagnetic ground state such as the $[4Fe-4S]^{2+}$ and $[2Fe-2S]^{2+}$ forms of iron−sulfur proteins and peroxodiiron(III) and diiron(IV) intermediates formed during O_2 activation by non-heme diiron proteins, which are not amenable to detection by the more established RFQ EPR method, are readily detected and quantified by Mössbauer spectroscopy. Thus, the kinetics of an iron enzyme *in a single turnover* can be defined. In the least auspicious case, the disappearance of Fe-containing reactants and formation of Fe products are directly reported. In the best case, new intermediates are detected, their oxidation and spin states are defined, and their kinetics of formation and decay are revealed. In one case, RFQ Mössbauer spectroscopy has been used to resolve the isotope-sensitive step in a reaction involving cleavage of an unactivated C−H bond, allowing for direct determination of the intrinsic deuterium kinetic isotope effect. In other cases, the formation of amino acid radicals has been demonstrated by Mössbauer spectroscopy by virtue of their dipolar coupling with a nearby paramagnetic iron center. The advent of γ-radiolytic cryoreduction has made it possible to interconvert odd- and even-electron centers, providing a valuable tool for establishing the net oxidation states of new intermediates and permitting interrogation of initially integer-spin or diamagnetic centers by EPR and more advanced electron magnetic resonance methods (e.g., ENDOR). In the latter application, as in the use of RFQ with other spectroscopies to characterize new iron complexes, Mössbauer spectroscopy serves an essential quality-control function. Perhaps the most exciting recent development, however, is the prediction of Mössbauer parameters using DFT methods. The sensitivity of the Mössbauer parameters to details of the structure permits high-resolution structural information for new intermediates to be extracted. For example, Mössbauer parameters calculated from a DFT-derived structure of **J**, the Fe(IV)═O^{2-} intermediate from the TauD catalytic cycle, agree well with the experimental parameters. The structure is also consistent with the Fe═O distance defined in EXAFS experiments. These notable consistencies inspire confidence that the DFT-derived structure is likely to be essentially correct. Given that Mössbauer spectroscopy has played a pivotal role in the detection of novel iron intermediates, the potential to evaluate high-resolution models of a new complex derived from DFT by comparison of calculated and experimental Mössbauer parameters is exciting indeed.

Acknowledgment. These studies have been supported by the Pennsylvania State University (start-up funds to M.T.G. and C.K.) and the National Institutes of Health [NIH-GM 55365 (J.M.B.) and NIH-GM 69657 (J.M.B. and C.K.)]. We thank our collaborators and co-workers whose work is described in this article.

IC048523L